Approaching hydroelasticity of large vessels with multi-body dynamics

K. de Klerk

Technische Universiteit Delft

TU Delft

Allseas

Approaching hydroelasticity of large vessels with multi-body dynamics

by

K. de Klerk

to obtain the degree of Master of Science
at the Delft University of Technology,
to be defended publicly on Tuesday March 16, 2021 at 14:30.

Student number:	4383133	
Project duration:	April 20, 2020 – March 16, 2021	
Thesis committee:	Dr. ir. P.R. Wellens,	TU Delft, supervisor
	Dr. ir. L. Pahlavan,	TU Delft
	ir. P. Xu,	TU Delft
	ir. F. Rodenburg,	Allseas, daily supervisor
	ir. K. Aalbers,	Allseas, daily supervisor

TU Delft

Preface

This thesis has been written in fulfilment of the Masters degree Marine Technology at Delft University of Technology and was written at Allseas.

The enormous size of marine and offshore structures amazes me and is the main reason why I decided to study Marine Technology at the Delft University of Technology. At the beginning of my study the build of the largest vessel in the world was completed and first arrived in the port of Rotterdam. I am grateful that I had the opportunity to write my thesis at Allseas about this enormous vessel: Pioneering Spirit.

I especially would like to thank Freek and Kees, my daily company supervisors, for helping me through the process of graduating and their enthusiasm for this graduation topic. Due to the Covid measurements working from home was the new standard, which is not ideal when you are graduating at a company, but because of all the online meetings and coffee talks they made it quite easy to discuss the progress and receive helpful feedback.
I also would like to thank Peter, my supervisor from TU Delft, for keeping me on the right track during this entire graduation process and sharing his expertise with me.
Finally, I would like to thank everyone else who has supported me during this entire graduation process.

K. de Klerk
Delft, March 2021

Abstract

The size of vessels has increased significantly over the last decades and will increase even further in the decades to come. This trend is mainly visible in the size of container ships. A decade ago the largest container ship had a capacity of 13.500 TEU, nowadays the largest container ship has a capacity of almost 24.000 TEU. The capacity of the largest container ship has almost doubled in only one decade. Due to their increasing size, vessels tend to become more flexible and their structural natural frequencies move towards the range of typical wave frequencies. Excitation of these structural modes will lead to resonant hull vibrations.

The traditional method to determine wave loads and the response of vessels due to these wave loads is based on the assumption that the vessel acts as a rigid body. For large vessels, which tend to be more flexible, this is not a reliable method. A method is required that takes into account the fluid-structure interaction, which is in this case called hydroelasticity. The most used method to approach hydroelasticity is based on modal decomposition and was first established by Bishop & Price in 1979. Since then, this method has been developed into commercial software and is nowadays accessible to the industry. However, the currently available commercial software is limited to first order hydroelasticity.

Larger vessels become more flexible, but even the largest vessels still have their first structural natural frequency above the range of typical wave frequencies. It is thus very unlikely that first order theory can explain the excitation of these structural modes. However, several evidences of resonance around the wet natural frequencies have been reported. The structural modes could be excited by second order wave loads. Second order wave loads contain sum-frequency terms that occur at higher frequencies than the encountered wave frequencies. These second order wave loads have been considered for elastic bodies by including these loads in the method based on modal decomposition. It is expected that the second order hydroelastic response has a significant contribution to the total response for very large vessels.

Pioneering Spirit is currently the largest construction vessel in the world. The vessel is designed for the single-lift installation and removal of large oil and gas platforms. A correct prediction of the response of this vessel requires a hydroelastic analysis. The vessel has its structural natural frequencies far above the range of expected wave frequencies, but evidences of resonance around the wet natural frequencies have been reported for this vessel. This research focuses on explaining the observed response by considering second order wave loads.

The second order hydroelastic response is obtained with the method based on modal decomposition with a non-commercial version of Hydrostar. It was found that the second order wave loads cause the observed high-frequent response of the vessel. The main disadvantage of this method is that the second order hydroelastic response can not be computed with the use of commercial software. This makes it impossible to predict the hydroelastic response of the vessel in the future for different drafts and loading conditions.

An alternative method is proposed to overcome this problem. This method is based on multi-body dynamics. The advantage of this method is that there is commercial software that can obtain second order wave loads for multiple interacting bodies. A multi-body model is created for Pioneering Spirit by dividing the vessel into a number of rigid bodies. These bodies are connected to each other by beam elements. The linear transfer functions obtained with this method are compared to the ones obtained with modal decomposition and show good agreement.

This multi-body model is then used to obtain the second order hydroelastic response of the vessel by calculating the second order wave loads and substituting these loads in the equation of motion. The second order hydroelastic response shows very little resemblance with the method based on modal decomposition and with the measured response. It is found that in the calculated second order wave loads, a part of the second order wave loads is missing. This part has a significant contribution to the sum-frequency terms of the second order wave loads according to a number of studies. Taking into account this missing part should lead to a more accurate approximation of the second order wave loads and eventually to a more accurate approximation of the second order hydroelastic response obtained with multi-body dynamics.

List of Figures

List of Tables

Contents

1

Introduction

The size of vessels has increased significantly over the last decades and will increase even further in the decades to come. This trend is mainly visible in the size of container ships. A decade ago the largest container ship had a capacity of 13.500 TEU, nowadays the largest container ship has a capacity of almost 24.000 TEU. The capacity of the largest container ship has almost doubled in only one decade. Due to their increasing size, vessels tend to become more flexible and their structural natural frequencies move towards the range of typical wave frequencies. Excitation of these structural modes will lead to resonant hull vibrations.

Pioneering Spirit is the largest construction vessel in the world. The vessel is designed for the single-lift installation and removal of large oil and gas platforms. The vessel is 382 meters long and 124 meters wide and has quite an unconventional shape. The vessel actually consists of two hulls that are merged together from the stern towards the deck house. This leaves a slot at the fore ship of the vessel, which is 122 meters long and 59 meters wide. This slot enables Pioneering Spirit to position itself around the platform and remove or install topsides in a single lift. The aft ship of the vessel is reserved for the Jacket Lift System, which will be used to remove and install jackets. This system consists of two 170 meters long lifting beams, which can rotate on hinges which will be located at the vessel's stern.

Figure 1.1: Pioneering Spirit carrying a topside

The traditional method for predicting the response of a vessel is based on the assumption that the vessel acts as a rigid body. This is a valid assumption when the deformations of the vessel are negligible. However, since ships tend to become more flexible this assumption is not valid anymore. Fluid-structure interaction (FSI) should be taken into account when predicting the response of these

large vessels. This response is generally known as the hydroelastic response and this hydroelastic response can be separated into springing and whipping. Springing refers to the global resonant hull vibrations induced by continuous wave loads. Whipping refers to the transient hull vibrations induced by impulsive loads such as wave slamming. This research will focus on springing of large vessels.

1.1. Background

The basic principle for hydroelasticity was first established in the seventies by Bishop and Price [3]. The structural behaviour of the hull was modelled with a Timoshenko beam and the hydrodynamics of the hull was captured with linear strip theory. In this approach the dynamic response of the hull is expressed in terms of the superposition of its dry natural modes, including the rigid body modes. These mode shapes are considered as the new basis of the system and the physical quantities as added mass, stiffness, damping and excitation force are expressed in this modal space. Together, the wet natural frequencies and transfer functions for the hydroelastic response to wave loads can be obtained. Nowadays, the structural behaviour of vessels can be modelled accurately with 3D-finite element models. There are multiple successful applications of 3D-finite element models in hydroelastic analysis based on modal decomposition [13, 15, 26].

Another method to deal with the hydroelastic response of elastic structures is based on multi-body dynamics [18, 28]. In this method the elastic structure is discretized into a number of rigid bodies which are connected by elements representing the stiffness of the elastic structure. This method does not require the pre-determination of mode shapes of an elastic structure, in contrast to method based on modal decomposition.

So far, most of the numerical methods have been focusing on obtaining the first order hydroelastic response, so only taking into account the linear quantities. The non-linear quantities that have been taken into account with these numerical methods are slamming forces and the non-linear Froude Krylov correction [19]. The natural frequencies of large vessels can be excited even when the encountered wave frequencies are significantly lower than the natural frequencies. Second order theory allows to calculate wave loads at higher frequencies than the encountered wave frequencies, possibly around the wet natural frequencies. Second order theory was proven to be successful in explaining the resonance motion observed at Tension Leg Platforms (TLP) [7]. TLP's typically have their natural frequency above the range of expected wave frequencies, but still resonance was observed in reality. Second order wave loads are seen as the primary source of these resonant motions.

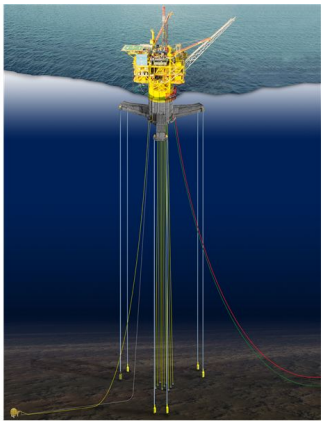

Figure 1.2: Schematic of a TLP

Only recently, second order wave loads have been considered for elastic bodies. The work that has been done so far for second order wave loads on elastic bodies is based on modal decomposition. Shao and Faltinsen [27] presented a time domain Higher Order Boundary Element Method to calculate the second order excitation force for the 2-node vertical bending mode of a Wigley hull. They formulated the Boundary Value Problem to solve the potentials in a body-fixed coordinate system instead of an inertial coordinate system and found that the second order potential has a great contribution to the second order excitation force. Heo and Kashiwagi [12] proposed a numerical method to calculate the second order excitation force based on a direct time-domain Rankine panel method. They found as well that the second order potential has a great contribution to the second order excitation force with respect to the contribution coming from the first order response. Choi [8] solved the second-order hydrodynamic force and response for a bottom-mounted elastic cylinder based on the semi-analytical modal decomposition method. Malenica [22] used this method to consider the second order boundary value problem of an elastic body. This method was implemented in the hydrodynamic solver Hydrostar

and was validated with the results from Choi [8].

1.2. Gap analysis: considering second order wave loads in a hydroelastic method based on multi-body dynamics

It is expected that the size of ships will keep increasing and for these large vessels hydroelasticity will play an important role. The most commonly used method to approach hydroelasticity is based on modal decomposition. There are multiple successful applications of this method to approach the first order hydroelastic response of a vessel. However, it is unlikely that first order hydroelastic theory is able to explain a possible excitation at the natural frequencies of a large vessel. This is because even the largest vessels sailing this planet nowadays, still have their natural frequencies far above the range of typical wave frequencies. Second order wave loads should be considered when approaching hydroelasticity of large vessels, since it are these loads that can excite the natural frequencies in an ordinary wave spectrum.
So far, second order wave loads have been considered in a few studies to approach hydroelasticity. In all these studies hydroelasticity is approached with modal decomposition. The other method to approach hydroelasticity is based on multi-body dynamics. This method has mainly been studied to approach hydroelasticity of Very Large Floating Structures. Within these studies only the first order hydroelastic response has been considered. Approaching hydroelasticity with multi-body dynamics and considering second order wave loads could lead to an accessible and realistic approximation of the hydroelastic response for large vessels.

1.3. Problem statement

Pioneering Spirit is currently the largest vessel in the world, assuming that it acts as a rigid body is not sufficient enough anymore to predict the response of the vessel. Figure 1.3 shows the measured vertical acceleration in one of the bows and the prediction based on a rigid body assumption (referred to as hydro-structural prediction in figure 1.3). It can be seen that the measured response exceeds the prediction. Post-processing the time-signal reveals that there is a significant high-frequent response present, as can be seen in figure 1.4.
Considering the vessel as an elastic body could lead to a better prediction of the total response of the vessel. The high-frequent response occurs between □ and □ rad/s. A typical wave spectrum does not contain much wave energy around these frequencies, which makes it unlikely that the high-frequent response can be explained with first order wave loads. Second order wave loads should be considered as the source of the high-frequent response of Pioneering Spirit.

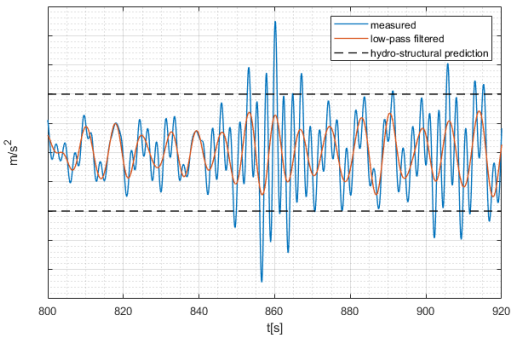

Figure 1.3: Vertical acceleration measured on board of Pioneering Spirit

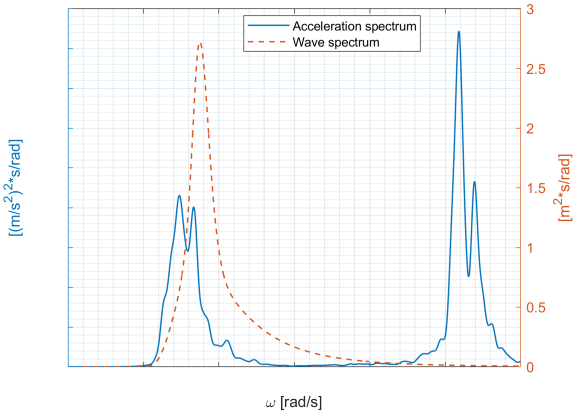

Figure 1.4: Measured acceleration spectrum

Measured data of Pioneering Spirit has been studied to indicate the size of the problem. Pioneering Spirit is equipped with a large number of sensors and all of these sensors have been collecting data over the past years.
Figure 1.5 shows a part of a measured time series. This time series contains the measured vertical

acceleration in one of the bows. A low-pass filter is applied to this time signal with a cutoff frequency of □ Hz, around □ rad/s. This filtered signal is indicated with WF, which stands for wave-frequent part. The wave-frequent part of the response can be predicted very well by assuming that the vessel acts as a rigid body. The time series is divided into cycles with the use of a zero up-crossing method and for each cycle the maximum and minimum of the wave-frequent response and the total response are obtained. The total response is plotted as a function of the wave-frequent response for each cycle and normalized by the maximum recorded response in figure 1.6.
The green line represents cycles in which the high-frequent response has almost no contribution to the total response. The yellow and pink lines represent cycles in which the total response is respectively 2 and 6 times higher than the wave-frequent part. It was found that for at least 40% of the recorded cycles the total response is at least 2 times higher than the wave frequent response.
The high-frequent response can have a significant contribution to the total response of the vessel. Therefore, it is important that this high-frequent response is predicted correctly.

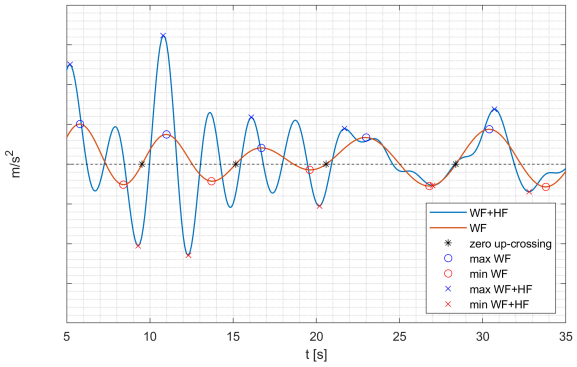

Figure 1.5: Time series divided into cycles.

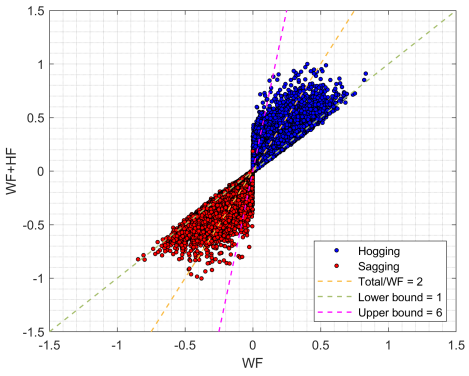

Figure 1.6: Total response as a function of the wave-frequent response for all recorded cycles

1.4. Objective

The first objective of this thesis is to find an explanation for the observed high-frequent response of Pioneering Spirit by considering the vessel as an elastic body and consider continuous wave loads. It is unlikely that the observed high-frequent response is caused by first order wave loads and it is expected that second order wave loads cause the observed high-frequent response. The first and second order hydroelastic response will be approached with the method based on modal decomposition and the method based on multi-body dynamics. The second order hydroelastic response will be calculated with a version of Hydrostar that includes the numerical code from Malenicia [22].
If second order wave loads can explain the observed high-frequent response, then how can this response be predicted in the future. At this moment, no commercial version of Hydrostar is able to calculate the second order hydroelastic response with the method based on modal decomposition. So far, this method is the only method that has been used to approach the second order hydroelastic response. The method based on multi-body dynamics is considered far less when approaching hydroelasticity and hasn't been used yet to obtain the second order hydroelastic response. The second objective is to approach the second order hydroelastic response with the method based on multi-body dynamics as well. A number of commercial hydrodynamic solvers has the feature to calculate second order wave loads for multiple interacting bodies. Combining one of those hydrodynamic solvers with the method based on multi-body dynamics, can be used to approach the second order hydroelastic response of the vessel and eventually predict the high-frequent response of the vessel in the future.

1.4.1. Hypotheses

The following two hypotheses are formulated to reach the objectives of this thesis.

Hypothesis 1 *The observed high-frequent response of Pioneering Spirit is caused by second order wave loads.*

Hypothesis 2 *The second order hydroelastic response of Pioneering Spirit can be approached using multi-body dynamics.*

1.5. Outline of the report

Chapter 2 and chapter 3 present the first and second order theory to approach hydroelasticity with both methods. These methods are both applied to Pioneering Spirit to obtain the first and second order hydroelastic response of the vessel. Chapter 4 presents the results coming from both methods and compares the results to the measured response of the vessel. Chapter 6 discusses the results and discusses if the hypotheses can be accepted or rejected. The final chapter includes the conclusions and recommendations of this thesis.

2

First order hydroelasticity

This chapter introduces both methods to approach hydroelasticity by presenting the first order theory for both methods. Next, it describes how both methods are applied to Pioneering Spirit to obtain the first order hydroelastic response of the vessel.

2.1. Modal decomposition

The method based on modal decomposition introduced by Bishop and Price [3] is a widely used method to approach hydroelasticity. A detailed description of this method is given in appendix A and a brief summary will be given here. This method approaches the dynamic response of an elastic body as a superposition of its modeshapes. This means that the deformation at any location of the vessel can be described by a superposition of a time dependent part and a space dependent part:

$$\vec{X}(x,y,z,t) = \sum_{j=1}^{N} \zeta_j e^{-\mathrm{i}\omega t} \vec{\delta}_j(x,y,z) \tag{2.1}$$

where X is the deformation anywhere on the vessel, N is the total number of modes taken into account, ζ_j is the modal amplitude and $\vec{\delta}_j$ is the j^{th} dry modeshape.
This method is used by Senjanovic & Malenica in [26] to estimate the springing response of an elastic barge considering first order wave loads. Their numerical results show good agreement with the measured response of the elastic barge.

First the dry natural frequencies and modeshapes ($\vec{\delta}_j$) of the vessel are obtained. This can be done using a three dimensional finite element model, but for beam-like hulls it can be convenient to use a one dimensional finite element model. The modeshapes of the vessel form the new basis of the system and the physical quantities are determined in the modal space.

The modes are transferred to the geometry of the wetted surface of the vessel, which is generally represented in a panel model. The dry modeshape mapped on the panel model is denoted with h_j. Because modal decomposition is assumed, the deformation of the wetted surface can be presented as:

$$\vec{H}(x,y,z,t) = \sum_{j=1}^{N} \zeta_j e^{-\mathrm{i}\omega t} \vec{h}_j(x,y,z) \tag{2.2}$$

where $H(\vec{x},t)$ is the vector for the deformation of the wetted surface, ζ_j is the modal amplitude and $h_j(\vec{x})$ is a vector containing the j^{th} dry modeshape transferred from the structural model to the wetted surface.
The linear potential theory is used to describe fluid motion and calculate the hydrodynamic loads. The hydrodynamic part obtains the physical terms as added mass, hydrodynamic damping and excitation force per mode.

By collecting the hydrodynamic terms and including the modal mass and stiffness coming from the structural part, the modal equation of motion become:.

$$(-\omega^2([M]+[A]) - \mathrm{i}\omega[B] + [K] + [C])\vec{\zeta} = \vec{F} \tag{2.3}$$

Solving the modal equation of motion leads to the modal amplitudes ζ_j. These modal amplitudes are substituted into equation 2.1 to obtain the first order hydroelastic response at any location of the vessel. Because the first order response is periodic with frequency ω, the local velocity and local acceleration can be derived as follows:

$$\begin{aligned} \vec{X}(x,y,z,t) &= \sum_{j=1}^{N} \zeta_j e^{-\mathrm{i}\omega t}\vec{\delta}_j(x,y,z) \\ \frac{\partial \vec{X}}{\partial t} &= -\mathrm{i}\omega \sum_{j=1}^{N} \zeta_j e^{-\mathrm{i}\omega t}\vec{\delta}_j = -\mathrm{i}\omega\vec{X} \\ \frac{\partial^2 \vec{X}}{\partial t^2} &= -\omega^2 \sum_{j=1}^{N} \zeta_j e^{-\mathrm{i}\omega t}\vec{\delta}_j = -\omega^2\vec{X} \end{aligned} \tag{2.4}$$

2.1.1. Application to Pioneering Spirit

The first order hydroelastic response based on modal decomposition is obtained with the software package HOMER. A three dimensional finite element model is used to obtain the dry natural frequencies and modeshapes. Only the first two structural modes are taken into account in the hydroelastic analysis. More structural modes could be taken into account as well, but the first following structural modes have a natural frequency significantly higher than the considered structural modes and require a much finer mesh which will lead to an increase in the computational time.

Table 2.1: Dry natural frequencies from the finite element model, mode 1-6 are rigid body modes

	FEM
Mode 7	☐ Hz
Mode 8	☐ Hz
Mode 9	☐ Hz
Mode 10	☐ Hz

The dry modes are mapped onto the geometry of the wetted surface as can be seen in figures 2.1 and 2.2. A total of 15,244 diffracting elements is used to mesh the wetted surface. HOMER calculates the hydrodynamic terms for the rigid body modes and the first two structural modes and solves the equation of motion to obtain the modal amplitude.

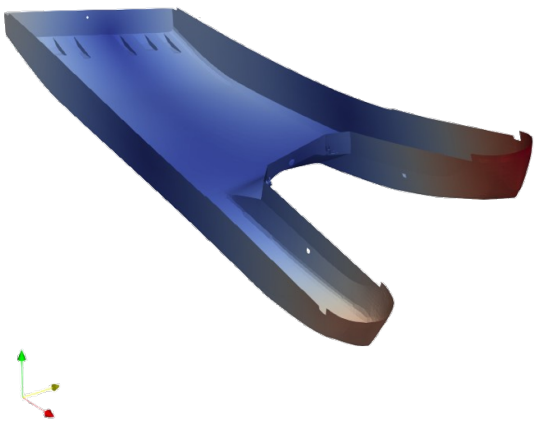

Figure 2.1: Mode 7

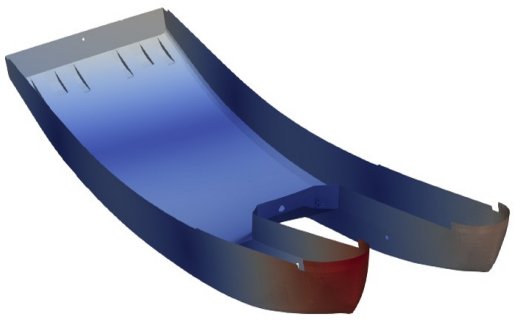

Figure 2.2: Mode 8

The modal amplitudes are obtained for wave frequencies from □ to □ rad/s and for incoming wave directions from $0°$ to $360°$ with an interval of $15°$. Figures 2.3 and 2.4 show the response amplitude operators for the modal amplitudes of the first and second structural mode. These structural modes will be excited by waves with frequencies between □ and □ rad/s. The modal amplitudes are eventually transformed into local displacements, velocities and accelerations with equation 2.4.

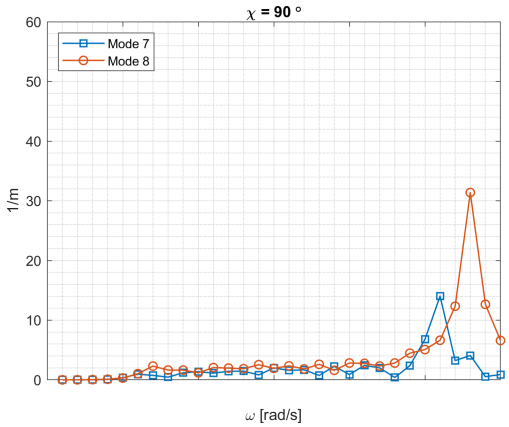

Figure 2.3: RAO mode 7 and 8, $\chi = 90°$

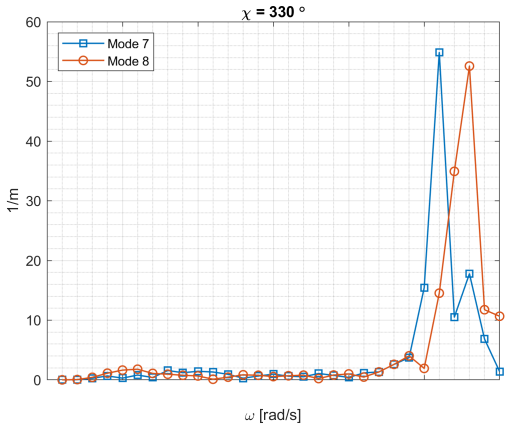

Figure 2.4: RAO mode 7 and 8, $\chi = 330°$

2.2. Multi-body dynamics

The method to approach hydroelasticity with multi-body dynamics was proposed by Lu [18] to approach the hydroelasticity of a Very Large Floating Structure.
In this method the continuous elastic body is divided into a number of rigid bodies connected to each other using beam elements as is illustrated in figure 2.5. For this method the linear potential theory is adopted as well, to calculate hydrodynamic loads on multiple interacting rigid bodes.

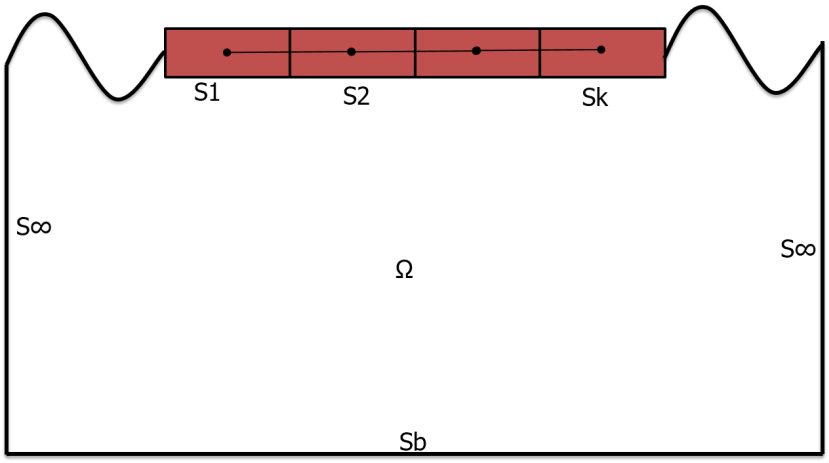

Figure 2.5: Continuous flexible structure discretized to multiple rigid bodies connected with flexible beam elements

Similar boundary conditions apply for multiple interacting rigid bodies as for a single rigid body. These are the well known boundary conditions as satisfying the Laplace equation, the free surface boundary condition, the seabed boundary condition and the body boundary condition. In the case of multiple interacting bodies, the body boundary condition is defined for each body separately, where each body is indicated with k:

$$\frac{\partial \phi}{\partial n_k} = \vec{V}_k \cdot \vec{n}_k \tag{2.5}$$

The linear velocity potential is decomposed into an incident, diffraction and radiation potential. In the case of multiple interacting bodies, the total number of degrees of freedom is $6xM$, where M is the total number of bodies. The linear velocity potential is then expressed as:

$$\phi(x,y,z,t) = \varphi(x,y,z)e^{-\mathrm{i}\omega t} = \left[(\varphi_I + \varphi_D) - \mathrm{i}\omega \sum_{m=1}^{M}\sum_{j=1}^{6} \varphi_{Rjm} x_{jm}\right] e^{-\mathrm{i}\omega t} \tag{2.6}$$

where φ_I is the space dependent part of the incident potential, φ_D of the diffraction potential, x_{jm} is the amplitude of the motion of the j^{th} degree of freedom of the m^{th} body and φ_{Rjm} is the radiation potential due to the j^{th} motion of the m^{th} body. In the first order theory the linearized Bernoulli equation is used to calculate the pressures.

$$p = -\rho g z - \rho \frac{\partial \phi}{\partial t} \tag{2.7}$$

The pressures are integrated over the wetted surface of each body to calculate the loads acting on each body. The excitation loads acting on each structure are given by:

$$\vec{F}_{Ek} = \left[\mathrm{i}\omega\rho \iint_{S_k} (\varphi_I + \varphi_D) \cdot \vec{n}_k \cdot dS\right] e^{-\mathrm{i}\omega t} \tag{2.8}$$

The radiation potential results in the added mass and hydrodynamic damping of each body, these terms

are given by:

$$[A_{km}] = \rho Re\left\{\iint_{S_k} \varphi_{Rm} \cdot \vec{n}_k \cdot dS\right\}$$
$$[B_{km}] = \rho\omega Im\left\{\iint_{S_k} \varphi_{Rm} \cdot \vec{n}_k \cdot dS\right\} \tag{2.9}$$

The mass of each body is represented as a lumped mass, so the mass of the entire structure is described in a lumped mass matrix. Collecting the masses, hydrodynamic terms and wave loads for each body results in an equation of motion for multiple interacting bodies:

$$\left\{-\omega^2\left(\begin{bmatrix} M_{1,1} & \dots & 0 \\ \vdots & \ddots & \\ 0 & & M_{M,M} \end{bmatrix} + \begin{bmatrix} A_{1,1} & \dots & A_{1,M} \\ \vdots & \ddots & \\ A_{M,M} & & A_{M,M} \end{bmatrix}\right) - \mathrm{i}\omega \begin{bmatrix} B_{1,1} & \dots & B_{1,M} \\ \vdots & \ddots & \\ B_{M,M} & & B_{M,M} \end{bmatrix} + \begin{bmatrix} C_{1,1} & \dots & 0 \\ \vdots & \ddots & \\ 0 & & C_{M,M} \end{bmatrix}\right\} \begin{Bmatrix} \vec{X}_1 \\ \vdots \\ \vec{X}_M \end{Bmatrix} = \begin{Bmatrix} \vec{F}_{E\,1} \\ \vdots \\ \vec{F}_{E\,M} \end{Bmatrix} \tag{2.10}$$

At this stage the bodies are only interacting with each other by the presence of water and not yet by the connection through the beam elements. The stiffness of the beam elements can easily be introduced into the equation of motion. The stiffness matrices of the beam elements transform the displacements at the nodes into forces:

$$\begin{Bmatrix} \vec{F}_1 \\ \vec{F}_2 \\ \vdots \\ \vec{F}_{M-1} \\ \vec{F}_M \end{Bmatrix} = \begin{bmatrix} K_{1,1} & K_{1,2} & \dots & 0 & 0 \\ K_{2,1} & K_{2,2} & \dots & 0 & 0 \\ \vdots & \vdots & \ddots & \vdots & \vdots \\ 0 & 0 & \dots & K_{M-1,M-1} & K_{M-1,M} \\ 0 & 0 & \dots & K_{M,M-1} & K_{M,M} \end{bmatrix} \begin{Bmatrix} \vec{X}_1 \\ \vec{X}_2 \\ \vdots \\ \vec{X}_{M-1} \\ \vec{X}_M \end{Bmatrix} \tag{2.11}$$

The method to construct a global stiffness matrix for multiple connected beam elements is explained in appendix D. Including the stiffness matrix in the equation of motion results in an equation of motion for the connected bodies.

$$\left\{-\omega^2([M] + [A]) - \mathrm{i}\omega[B] + [C] + [K]\right\}\vec{X} = \vec{F}_E \tag{2.12}$$

Solving this equation of motion leads to the hydroelastic response of the structure. Since it is assumed that each body acts as a rigid body, the response of each body can be transformed to any location on the structure with a simple transformation matrix [16]. As mentioned earlier, because the first order response is periodic with frequency ω, the velocity and acceleration can be derived from the motions of the bodies.

$$\frac{\partial \vec{X}}{\partial t} = -\mathrm{i}\omega\vec{X}$$
$$\frac{\partial^2 \vec{X}}{\partial t^2} = -\omega^2\vec{X} \tag{2.13}$$

Solving the linear velocity potential and eventually the equation of motion for multiple interacting bodies is a feature which many hydrodynamic solvers are capable of. Both AQWA and Hydrostar are even capable of including the stiffness matrix when solving the equation of motion. Before applying this method to Pioneering Spirit, a benchmark study is performed with AQWA to validate that the method is applied in the right way. The elastic barge from Senjanovic & Malenica [26] is modelled in AQWA and the results can be found in appendix C.

2.2.1. Application to Pioneering Spirit

A multi-body model of Pioneering Spirit is created by splitting the vessel into 8 rigid bodies, as can be seen in figures 2.6 and 2.7. The first two structural modes are a vertical bending mode and a torsional mode. The vessel is split into a minimum number of bodies that can reproduce these modes.

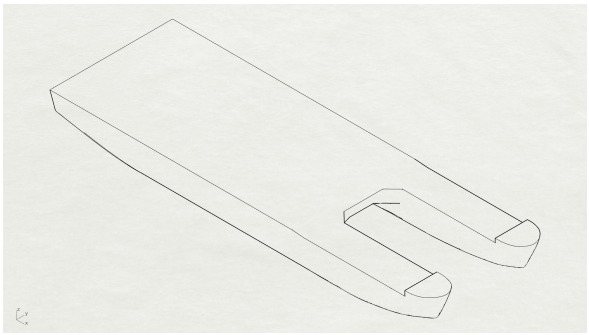

Figure 2.6: Hull Pioneering Spirit

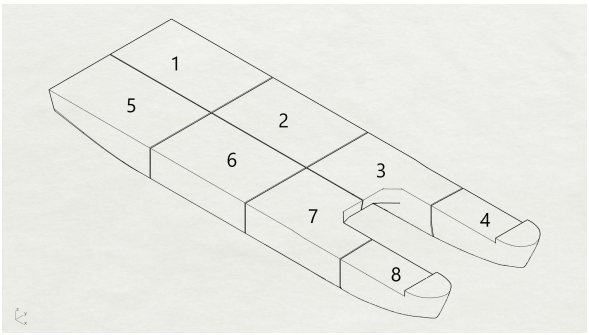

Figure 2.7: Pioneering Spirit divided into 8 rigid bodies

Structural model
The rigid bodies are connected to each other with a stiffness matrix. The vessel is divided into 8 rigid bodies and each body has 6 degrees of freedom, which means that the multi-body model has 48 degrees of freedom. The most accurate representation of the stiffness of the vessel is given by a finite element model of the vessel. This finite element model has more than 300,000 nodes, each with 6 degrees of freedom.
Numerous model reduction techniques exist in the field of structural dynamics [2, 9]. These techniques are capable of reducing the mass and stiffness matrix of a large finite element model to a small number of degrees of freedom. In this case there is chosen to reduce the finite element model in a much simpler way instead of applying one of the more sophisticated reduction techniques. The stiffness of the vessel will be represented in a finite element model consisting of beam elements. This model will be referred to as the beam model, whereas the complete finite element model, the one with more 300,000 nodes, will be referred to as the finite element model.

The beam model consists of 8 nodes, where each node represents a rigid body. The nodes are placed into the XY-plane and at a height of $z = 0.5D$, where D is the depth of the vessel (the distance between keel and deck). The nodes are connected to each other with a total of 10 beam elements as can be seen in figure 2.8.

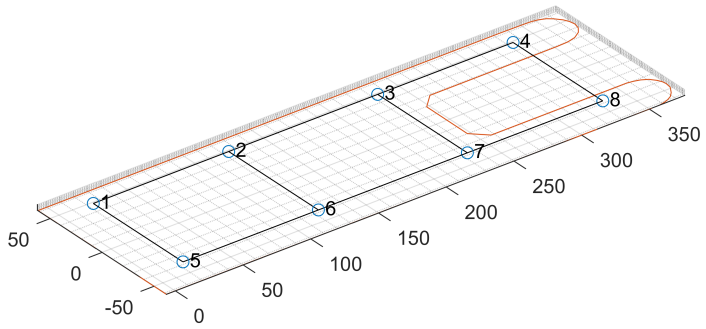

Figure 2.8: Structural model

The beam model contains two types of cross-sections. The longitudinal beam elements contain rectangular open cross-sections (figure 2.9). An open cross section comes close to the local cross

section of the hull. The width and the height of the open cross-section are based on the width and height of each body. The thicknesses of the web and flange are based on the thicknesses of the longitudinal bulkheads and decks. These thicknesses are fine tuned by hand, by means of trial and error, until the first two dry natural frequencies from the beam model match the dry natural frequencies from the finite element model. The transverse beam elements contain closed rectangular cross-sections (figure 2.10).
The beams are relatively short in length compared to their width and height. This means that shear deformation should be taken into account. Unlike Euler-Bernoulli beam theory, Timoshenko beam theory does take into account the shear deformation effects. Euler-Bernoulli beam theory is more suitable for slender beams. The global stiffness matrix is constructed from the separate beam elements. This global stiffness matrix is then transformed from the nodal coordinates to the centres of gravity of the rigid bodies. This is done because the hydrodynamic properties of the bodies will be determined in the centre of gravity of each body and the nodes don't coincide with these centres of gravity. An explanation on how the stiffness matrix is transformed is given in appendix C.

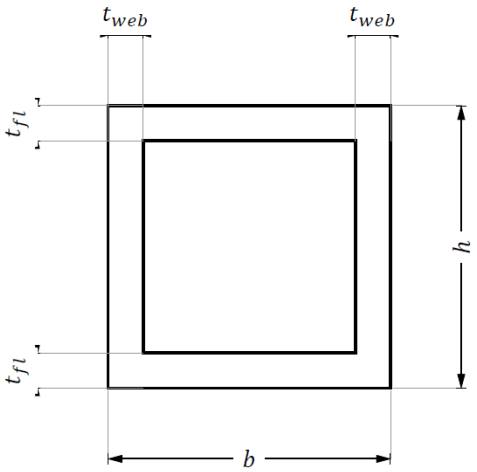

Figure 2.9: Open cross-section

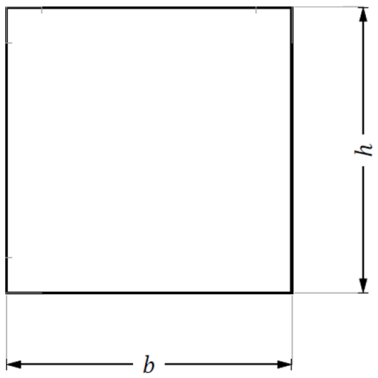

Figure 2.10: Closed cross-section

The mass of the vessel is represented into a lumped mass model. The mass distribution of the vessel is given in figure 2.11. This mass distribution is used to obtain the mass and inertia per body and is represented into a lumped mass matrix.

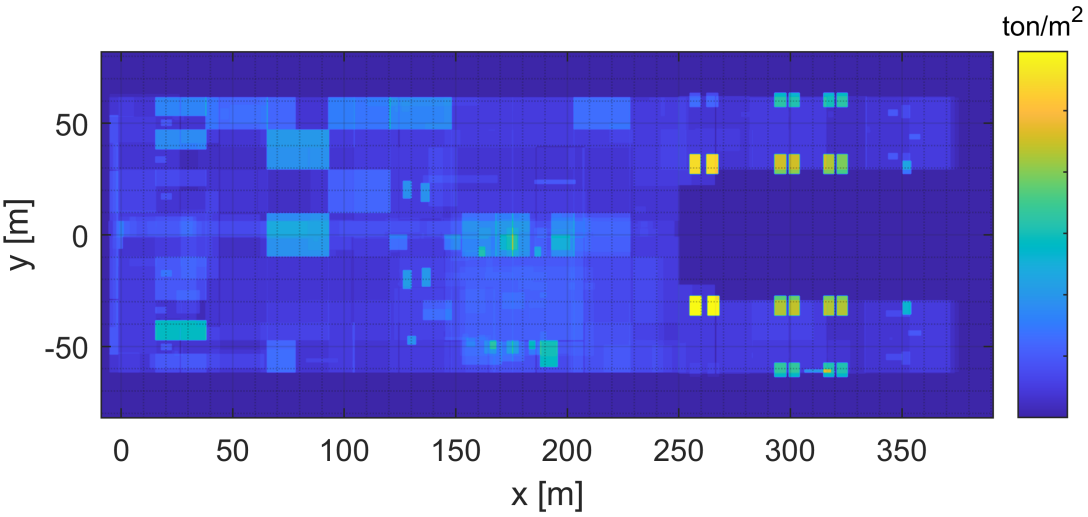

Figure 2.11: Distribution of the mass over the length and width of the vessel

Dry natural frequencies

The lumped mass matrix and stiffness matrix are used to obtain the dry natural frequencies of the beam model. The dimensions of the beam elements were fine tuned by hand until the first two dry natural frequencies from the beam model matched the first two dry natural frequencies from the finite element model. Table 2.2 shows the error in dry natural frequencies between the beam model and the finite element model. It can be seen that for the first two modes the error is less than one percent.

Table 2.2: Comparison of dry natural frequencies

	FEM	**Beam model**	**Error**
Mode 7	☐ Hz	☐ Hz	0.93 %
Mode 8	☐ Hz	☐ Hz	0.64 %

Figure 2.12 shows the modeshapes coming from the beam model, whereas figures 2.13 and 2.14 show the modeshapes coming from the finite element model. At first sight it looks as if the modeshapes coming from the beam model show a high correlation with the modeshapes coming from the finite element model. A practical method to measure the correlation between modeshapes is the Modal Assurance Criterion [23]. The Modal Assurance Criterion is bounded between 0 and 1, where 0 indicates no correlation and 1 indicates a high correlation between the modeshapes. Figure 2.15 shows this Modal Assurance Criterion between modes coming from the beam model and modes coming from the finite element model. It can be seen that for both modeshapes the criterion is close to 1, which indicates that there is a high correlation between the modeshapes coming from the beam model and the finite element model. The beam model is able to represent the global elastic behaviour of the vessel.

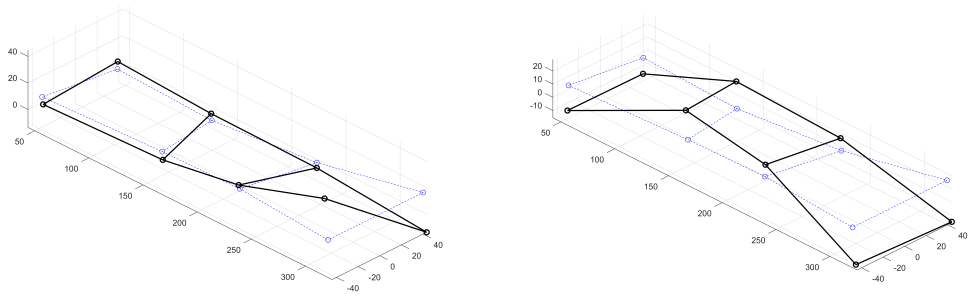

Figure 2.12: Mode 7 and 8 coming from the beam model

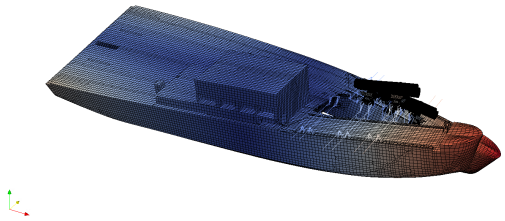

Figure 2.13: FEM mode 7, f_n = □Hz

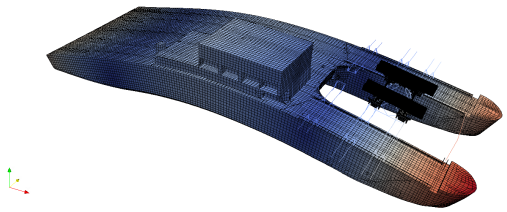

Figure 2.14: FEM mode 8, f_n = □Hz

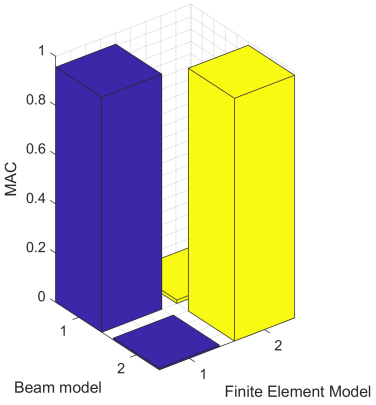

Figure 2.15: Modal Assurance Criterion for mode 7 and 8

Hydrodynamic model

The hydrodynamic terms are collected for each rigid body. According to the method based on modal decomposition the natural modes are excited by wave with a frequency between □ and □ rad/s. The hydrodynamic terms should thus be obtained for wave frequencies up to □ rad/s to capture the excitation by first order wave loads.

The geometry of the hull is divided into multiple bodies and this geometry is used to create a mesh for the multi-body analysis. This multi-body hydrodynamic analysis is performed in Hydrostar instead of AQWA. This is because AQWA requires a minimal number of elements per wavelength. For Pioneering Spirit this results in a maximum allowable wave frequency of □ rad/s with the maximum number of elements. Hydrostar doesn't have this limitation, which allows Hydrostar to solve for higher wave frequencies. The mesh that is used has a total of 15,496 diffracting elements, which is a similar mesh size as the mesh used for modal decomposition. Extra attention is paid to the fact that the added mass and hydrodynamic damping terms should converge moving towards these higher frequencies.

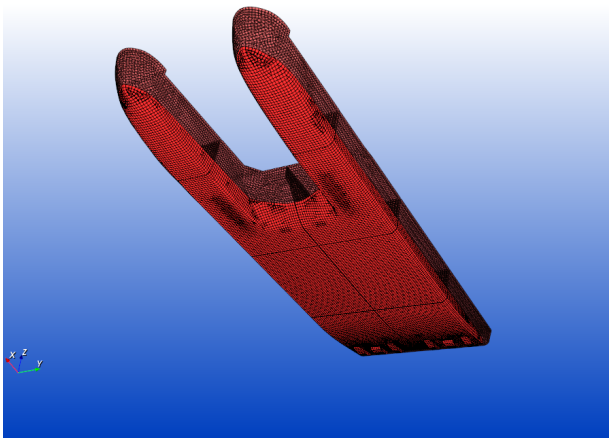

Figure 2.16: Mesh used for multi-body analysis

Figure 2.17 shows the response amplitude operators for the vertical acceleration of each body. can be seen that the natural modes will be excited when encountering waves with frequencies of approxi-

mately □ rad/s. This will result in high accelerations in the bows of the vessel. The RAO's of the bows are indicated with P4 and P8.

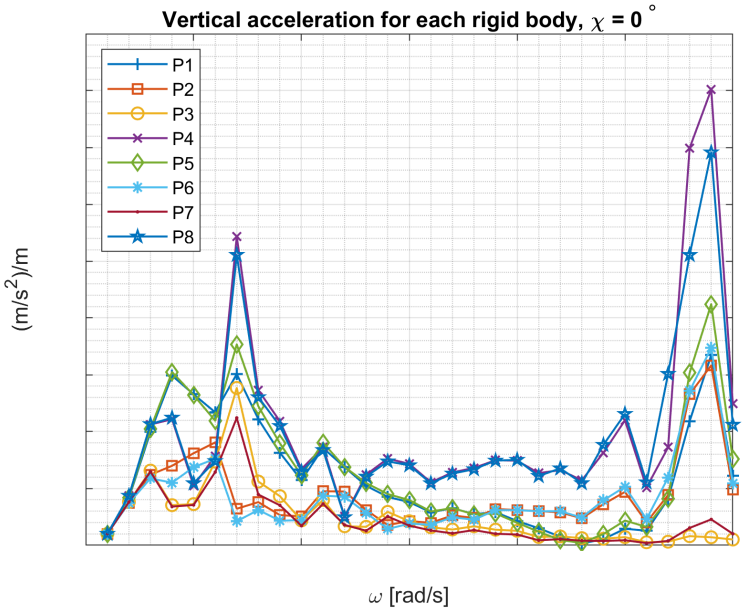

Figure 2.17: RAO's for vertical acceleration of each body

2.3. Summary

Both methods can be described as model order reduction techniques, because both method reduce the degrees of freedom of the elastic body. Modal decomposition is a popular model order reduction technique within structural dynamics [2]. The elastic response of the vessel is reduced to a superposition of its natural modes, including the rigid body modes. This model order reduction simplifies the hydrodynamic problem, because the velocity potential only has to be solved for the rigid body modes and a number of structural modes.
The method based on multi-body dynamics discretizes the elastic body into a number of rigid bodies, which reduces the degrees of freedom of the wetted surface as well and eventually simplifies solving the velocity potential.
The difference in model order reduction techniques and how these techniques reduce the degrees of freedom within the hydrodynamic model can be seen in the decomposition of the velocity potential for both methods.

Modal decomposition	**Multi-body dynamics**
$\varphi = \varphi_I + \varphi_D - \mathrm{i}\omega \sum_{j=1}^{N} \zeta_j \varphi_{Rj}$	$\varphi = \varphi_I + \varphi_D - \mathrm{i}\omega \sum_{m=1}^{M} \sum_{j=1}^{6} x_{jm} \varphi_{Rjm}$

Both methods approach the hydroelastic behaviour of the vessel in a different way. Modal decomposition requires the pre-determination of modeshapes, preferably with a three dimensional finite element model, and requires a hydrodynamic solver that can solve the velocity potential for generalized modes. The method based on multi-body dynamics does not require pre-determination of modeshapes and has the advantage that the mass and stiffness of the vessel can be adjusted quite easily without the need to recalculate the hydrodynamic terms as long as the geometry of the wetted surface remains the same. This makes the method based on multi-body dynamics very suited to approach hydroelasticity in the early design phase of large ships. Engineers do not have a very detailed finite element model at this early design phase, which is not needed for multi-body dynamics, and in this phase the structural properties of the vessel will be adjusted multiple times.

3

Second order hydroelasticity

The previous chapter explained the first order theory for both methods. This section will explain the second order theory for both methods. Extra attention is paid to how these second order methods are applied to Pioneering Spirit to obtain the second order hydroelastic response.

3.1. Modal decomposition

The method based on modal decomposition has been the only method yet to approach second order hydroelasticity. This method was described up to second order by Malenica [22]. This section will explain the theory and how it is applied to Pioneering Spirit.

The displacement of the wetted surface is described by vector $\vec{H}$, this vector can be described up to second order using a perturbation series:

$$\vec{H}(x,y,z,t) = \varepsilon\vec{H}^{(1)}(x,y,z,t) + \varepsilon^2\vec{H}^{(2)}(x,y,z,t) \tag{3.1}$$

Similar as for the first order theory, modal decomposition is adapted to split the vector $\vec{H}$ in a space dependent part and a time dependent part.

$$\begin{aligned}\vec{H}^{(1)}(x,y,z,t) &= \sum_{j=1}^{N} \zeta_j^{(1)} e^{-\mathrm{i}\omega t} \cdot \vec{h}_j(x,y,z) \\ \vec{H}^{(2)}(x,y,z,t) &= \sum_{j=1}^{N} \zeta_j^{(2)} e^{-\mathrm{i}(\omega_k+\omega_p)t} \cdot \vec{h}_j(x,y,z)\end{aligned} \tag{3.2}$$

The second order displacement vector is periodic with frequency $(\omega_k + \omega_p)$, because only the sum-frequent terms of the second order wave loads will be taken into account. The sum-frequent terms of the second order wave loads are periodic with $(\omega_k + \omega_p)$, which will be shown later on. The normal vector $\vec{N}$ of the wetted surface is decomposed into:

$$\begin{aligned}\vec{N} &= \vec{n} + \varepsilon\vec{N}^{(1)} \\ \vec{N}^{(1)} &= (\vec{\nabla}\cdot\vec{H}^{(1)})\vec{n} - [\vec{\nabla}\vec{H}^{(1)}]^T \cdot \vec{n}\end{aligned} \tag{3.3}$$

The derivation of $\vec{N}^{(1)}$ is given by Riggs & Huang [14], but can simply be seen as the variation of the normal vector due to the first order hydroelastic response of the body.

Second order potential

In order to determine the second order wave loads, the velocity potential is required. The velocity potential is described up to second order by using a perturbation series as well.

$$\phi = \varepsilon\phi^{(1)} + \varepsilon^2\phi^{(2)} \tag{3.4}$$

Describing the velocity potential up to second order, leads to an extra number of boundary conditions that need to be fulfilled. The second order potential needs to satisfy the same number and types of boundary conditions as the first order potential.
The free surface boundary condition for the second order potential, which states that the particles at the free surface should stay at the free surface and that the pressure is constant at the free surface, is given by:

$$\frac{\partial^2\phi^{(2)}}{\partial t^2} + g\frac{\partial\phi^{(2)}}{\partial z} = -2\left(\vec{\nabla}\phi^{(1)} \cdot \vec{\nabla}\frac{\partial\phi^{(1)}}{\partial t}\right) + \frac{\partial\phi^{(1)}}{\partial t} \cdot \left(\frac{\partial^2\phi^{(1)}}{\partial z^2} + \frac{1}{g} \cdot \frac{\partial^3\phi^{(1)}}{\partial t^2\,\partial z}\right) \tag{3.5}$$

At the body boundary there is a no-leak condition, stating that the fluid doesn't penetrate trough the body. This means that the velocity of the fluid at the body should be equal to the velocity of the oscillating body. For the second order potential this leads to the following body boundary condition:

$$\frac{\partial\phi^{(2)}}{\partial n} = -\left(\vec{\nabla}\vec{H}^{(1)} \cdot \vec{\nabla}\phi^{(1)}\right) \cdot \vec{n} + \left(\frac{\partial\vec{H}^{(1)}}{\partial t} - \vec{\nabla}\phi^{(1)}\right) \cdot \vec{N}^{(1)} \tag{3.6}$$

The forcing in the right-hand side of the second order free surface boundary condition is a quadratic function of the first order potential. The first order potential is periodic with frequency ω and given by:

$$\phi^{(1)}(x,y,z,t) = Re\left\{\varphi^{(1)}(x,y,z)e^{-\mathrm{i}\omega t}\right\} \tag{3.7}$$

If the sea is represented as a superposition of monochromatic waves, the treatment of the most general second order problem can be accomplished by treating the second-order free-surface condition as a bi-chromatic wave. The second order potential will take the following form:

$$\phi^{(2)}(x,y,z,t) = Re\left\{\varphi^{+(2)}(x,y,z)e^{-\mathrm{i}(\omega_k+\omega_p)t} + \varphi^{-(2)}(x,y,z)e^{-\mathrm{i}(\omega_k-\omega_p)t}\right\} \tag{3.8}$$

Due to the quadratic function of the first order potential, sum- and difference-frequency terms arise in the solution of the second order potential. For the same reason, sum- and difference frequency terms will also occur in the second order wave loads. The difference-frequency terms of the second order wave loads are what we know as wave drift loads, but we are interested in the sum-frequency terms. That is because it are these sum-frequency terms of the second order wave loads that can excite the natural modes of a large vessel. The difference-frequency terms of the second order potential will be neglected. The second order potential is decomposed into an incident potential and a diffraction potential.

$$\varphi^{+(2)}e^{-\mathrm{i}(\omega_k+\omega_p)t} = \left(\varphi_I^{+(2)} + \varphi_D^{+(2)}\right)e^{-\mathrm{i}(\omega_k+\omega_p)t} \tag{3.9}$$

The incident potential is known analytically, because this potential is independent of the presence of a body. This incident potential satisfies the Laplace equation, the seabed boundary condition and the free surface boundary condition.
The second order diffraction potential is chosen to satisfy the body boundary condition. Solving for this second order diffraction potential is described by Malenica [22] to be the main difficulty of solving the second order potential.

Pressure
After solving the second order potential, the pressures can be obtained by substituting the velocity potential into Bernoulli's equation (equation A.14). This will lead to a constant pressure, first order pressure and second order pressure.

$$\begin{aligned}
p &= p^{(0)} + \varepsilon p^{(1)} + \varepsilon^2 p^{(2)} \\
p^{(0)} &= -\rho g z \\
p^{(1)} &= -\rho g \vec{H}_3^{(1)} - \rho\frac{\partial\phi^{(1)}}{\partial t} \\
p^{(2)} &= -\frac{1}{2}\rho\left(\vec{\nabla}\phi^{(1)}\right)^2 - \rho\frac{\partial\phi^{(2)}}{\partial t} - \rho\left(\vec{H}^{(1)} \cdot \vec{\nabla}\frac{\partial\phi^{(1)}}{\partial t}\right)
\end{aligned} \tag{3.10}$$

where $H_3^{(1)}$ is the third entry of vector $H^{(1)}$.

Forces

The forces acting on the structure can be determined by integrating the pressure over the wetted surface S. Since we are interested in the modal forces, the pressures are projected onto the mode shapes:

$$F_j = \iint_S p \cdot \vec{h}_j \cdot \vec{N} \tag{3.11}$$

The wetted surface S is split into a constant part S_0 and a time varying part s, as can be seen in figure 3.1.

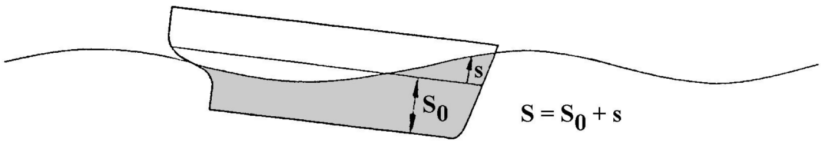

Figure 3.1: Wetted surface

The pressure and normal vector are substituted in equation 3.11. The following terms will eventually lead to second order wave loads:

$$\begin{aligned} F_j^{(2)} = &\iint_{S_0} p^{(1)} \cdot \vec{h}_j \cdot \vec{N}^{(1)} \cdot dS + \iint_{S_0} p^{(2)} \cdot \vec{h}_j \cdot \vec{n} \cdot dS \\ &+ \iint_s p^{(0)} \cdot \vec{h}_j \cdot \vec{N}^{(1)} \cdot dS + \iint_s p^{(1)} \cdot \vec{h}_j \cdot \vec{n} \cdot dS \end{aligned} \tag{3.12}$$

It should be noted that the time varying part s itself is already of first order. This means that integrating a first order term over this surface will lead to second order forces. The complete second order wave loads are given by:

$$\begin{aligned} F_j^{(2)} = &-\rho \iint_{S_0} \left(g\vec{H}_3^{(1)} + \frac{\partial \phi^{(1)}}{\partial t} \right) \cdot \vec{h}_j \cdot \vec{N}^{(1)} \cdot dS \\ &-\rho \iint_{S_0} \left(\frac{1}{2} (\vec{\nabla}\phi^{(1)})^2 + \vec{H}^{(1)} \cdot \vec{\nabla} \frac{\partial \phi^{(1)}}{\partial t} \right) \cdot \vec{h}_j \cdot \vec{n} \cdot dS \\ &-\rho \iint_{S_0} \frac{\partial \phi^{(2)}}{\partial t} \cdot \vec{h}_j \cdot \vec{n} \cdot dS \\ &-\rho g \iint_s z \cdot \vec{h}_j \cdot \vec{N}^{(1)} \cdot dS \\ &-\rho \iint_s \left(g\vec{H}_3^{(1)} + \frac{\partial \phi^{(1)}}{\partial t} \right) \cdot \vec{h}_j \cdot \vec{n} \cdot dS \end{aligned} \tag{3.13}$$

We can divide the second order wave loads into terms that originate from the second order potential ($F_{pj}^{(2)}$) and terms that originate from the quadratic function of first order terms ($F_{qj}^{(2)}$). The potential part of the second order wave loads is given by:

$$F_{pj}^{(2)} = -\rho \iint_{S_0} \frac{\partial \phi^{(2)}}{\partial t} \cdot \vec{h}_j \cdot \vec{n} \cdot dS \tag{3.14}$$

Since we are interested in the sum-frequent terms of the second order wave loads, this potential part is given by:

$$F_{pj}^{(2)} = \left(\mathrm{i}(\omega_k + \omega_p)\rho \iint_{S_0} \left(\varphi_I^{+(2)} + \varphi_D^{+(2)} \right) \cdot \vec{h}_j \cdot \vec{n} \cdot dS \right) e^{-\mathrm{i}(\omega_k + \omega_p)t} \tag{3.15}$$

The complete second order wave loads are given by:

$$F_j^{(2)} = F_{pj}^{(2)} + F_{qj}^{(2)} \tag{3.16}$$

Equation of Motion
Similar as for the first order theory, we can set up the equation of motion using Newton's second law. The second order wave loads are periodic with frequency $(\omega_k + \omega_p)$. The equation of motion for the modal structural model then becomes:

$$-(\omega_k + \omega_p)^2[M]\vec{\zeta}^{(2)}e^{-\mathrm{i}(\omega_k+\omega_p)t} = -[K]\vec{\zeta}^{(2)}e^{-\mathrm{i}(\omega_k+\omega_p)t} \tag{3.17}$$

where $\vec{\zeta}^{(2)}$ is a vector containing the second order modal amplitudes $\vec{\zeta}^{(2)} = \{\zeta_1^{(2)}, \zeta_2^{(2)}, \ldots \zeta_N^{(2)}\}$. The second order forces can be substituted into the above equation.

$$\begin{aligned}\left(-(\omega_k + \omega_p)^2[M] + [K]\right)\vec{\zeta}^{(2)}e^{-\mathrm{i}(\omega_k+\omega_p)t} &= \vec{F}^{(2)} \\ \left(-(\omega_k + \omega_p)^2([M] + [A]) - \mathrm{i}(\omega_k + \omega_p)[B] + [K] + [C]\right)\vec{\zeta}^{(2)} &= \vec{F}_E^{(2)}\end{aligned} \tag{3.18}$$

Solving the equation of motion for the modal amplitudes allows to obtain the second order hydroelastic response.

3.1.1. Application to Pioneering Spirit

The second order wave loads are obtained with a non-commercial version of Hydrostar that is used by Malenica in [22] and are provided by Bureau Veritas in the form of quadratic transfer functions.

The quadratic transfer functions contain the in- and out-of phase terms P^+ and Q^+, where the '+' notation indicates that the terms refer to the sum-frequent part of the second order wave loads. The second order wave loads follow from these terms as follows:

$$F_j^{(2)}(t) = \sum_{i=1}^{N}\sum_{j=1}^{N}\eta_i\eta_j(P_{ij}^+ + \mathrm{i}Q_{ij}^+)e^{-\mathrm{i}(\omega_i+\omega_j)t} \tag{3.19}$$

Where N is the number of wave components and η_i is the wave amplitude per wave component. Figure 3.2 shows the quadratic transfer function of $\left|T^+(\omega_i, \omega_j)\right|$ of the first two structural modes for an incoming wave direction of $30°$. $\left|T^+(\omega_i, \omega_j)\right|$ is the amplitude of the second order wave loads. The amplitude is a function of two wave frequencies, which are given on both axes. In this particular case, the highest second order wave loads occur around $\omega_1 \approx \square$, $\omega_2 \approx \square$ rad/s.

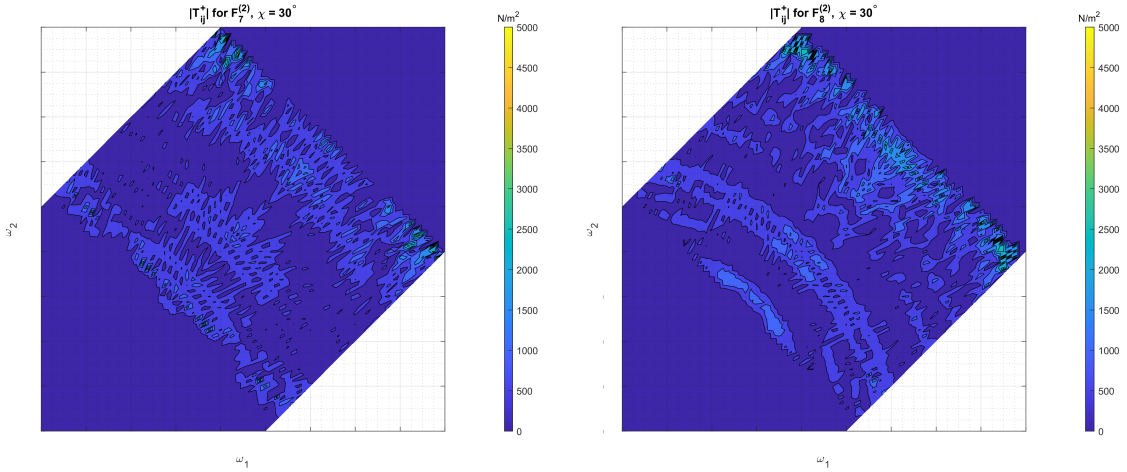

Figure 3.2: $|T^+|$ for mode 7 and 8 for an incoming wave direction of $\chi = 30°$

The second order wave loads are substituted into the equation of motion, equation 3.18, to solve for the modal amplitudes. These modal amplitudes are then used to obtain the second order hydroelastic response at any location on the vessel with:

$$\vec{X}^{(2)}(x, y, z, t) = \sum_{j=1}^{N}\zeta_j^{(2)}e^{-\mathrm{i}(\omega_i+\omega_j)t}\vec{\delta}_j(x, y, z) \tag{3.20}$$

Using the time dependent part in above equation, the local velocity and acceleration can be obtained.

$$\frac{\partial \vec{X}^{(2)}}{\partial t} = -\mathrm{i}(\omega_i + \omega_j)\vec{X}^{(2)}$$
$$\frac{\partial^2 \vec{X}^{(2)}}{\partial t^2} = -(\omega_i + \omega_j)^2 \vec{X}^{(2)} \tag{3.21}$$

The quadratic transfer function for the vertical acceleration at a specific point on the vessel is given in figure 3.3 for two different incoming wave directions. The wet natural frequencies of the vessel can be recognised in both figures. It seems that regular waves ($\omega_1 = \omega_2$) that result in sumfrequencies around the wet natural frequencies of the vessel cause the highest response.

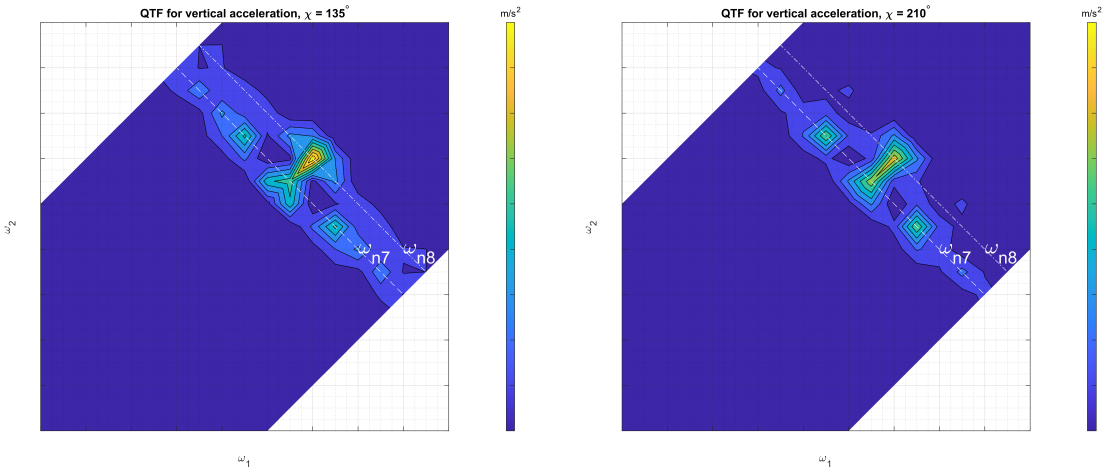

Figure 3.3: QTF for the vertical acceleration for, $\chi = 135°$ and $\chi = 210°$

The quadratic transfer functions are obtained for an incoming wave direction varying from $0°$ to $360°$ with an interval of $15°$. Using the quadratic transfer functions and a described wave spectrum it is possible to obtain a response spectrum. For this example a Jonswap spectrum is used to obtain the acceleration spectrum at a location in one of the bows. The following formula is used to transform a wave spectrum and quadratic transfer function into an acceleration spectrum [24].

$$S_{\ddot{H}_3^{(2)}}(\Omega) = 8\int_0^{\Omega/2} S(\omega)S(\Omega-\omega)\left|T_{\ddot{X}_3}(\omega,\Omega-\omega)\right|^2 \cdot d\omega \tag{3.22}$$

where Ω is the sumfrequency and $T_{\ddot{X}_3}$ is the quadratic transfer function for the vertical acceleration at the mentioned location. Figure 3.4 shows the acceleration spectrum for an incoming wave direction of $\chi = 135°$. It can be seen that the second order wave loads have a significant contribution to the total acceleration with respect to the first order wave loads.

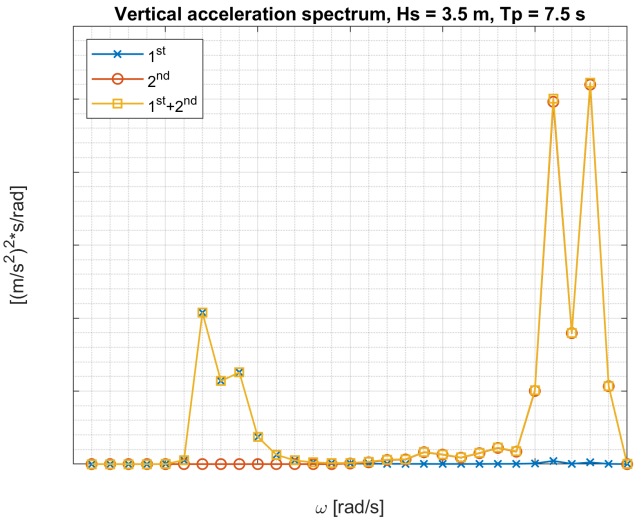

Figure 3.4: Acceleration spectrum containing $\ddot{X}_3^{(1)}$, $\ddot{X}_3^{(2)}$ and $\ddot{X}_3$

3.2. Multi-body dynamics

Second order wave loads on multiple interacting bodies have been studied in the past, especially for the hydrodynamics of cylindrical arrays [17, 20]. The computation of second order wave loads for a single rigid body is a well known procedure and can be achieved with multiple hydrodynamic solvers. Pinkster [24] first introduced a method to compute the second order wave loads based on direct pressure integration of all pressure contributions on the wetted surface of the vessel.
Similar as to the method based on modal decomposition, the velocity potential is described up to second order using a perturbation series. The second order body boundary condition for multiple interacting bodies is given by:

$$\vec{\nabla}\phi^{(2)} \cdot \vec{n}_k = -\left(\vec{X}_k^{(1)} \cdot \vec{\nabla}\right) \cdot \left(\vec{\nabla}\phi^{(1)} \cdot \vec{n}_k\right) + \left(\vec{V}_k^{(1)} - \vec{\nabla}\phi^{(1)}\right) \cdot \vec{N}_k^{(1)} \tag{3.23}$$

where $\vec{N}_k^{(1)}$ is the orientation of the normal vector due to first order motions. As mentioned before, the second order potential has the following form:

$$\phi^{(2)} = \varphi^{+(2)} e^{-\mathrm{i}(\omega_i+\omega_j)t} + \varphi^{-(2)} e^{-\mathrm{i}(\omega_i-\omega_j)t} \tag{3.24}$$

The sum-frequency terms of the second order wave loads are interesting in the case of hydroelasticity and this sum-frequent part is decomposed into an incident potential and a diffraction potential.

$$\varphi^{+(2)} = \varphi_I^{+(2)} + \varphi_D^{+(2)} \tag{3.25}$$

The second order incident potential is known analytically and is obtained by solving the boundary value problem in the absence of any body. Solving the entire boundary value problem will lead to the remaining second order potentials. Once the second order velocity potential is known, the second order wave loads can be calculated with direct pressure integration, where the pressure is obtained with the Bernoulli equation.

$$\begin{aligned} p^{(0)} &= -\rho g z \\ p^{(1)} &= -\rho g \vec{X}_3^{(1)} - \rho \frac{\partial \phi^{(1)}}{\partial t} \\ p^{(2)} &= -\frac{1}{2}\rho\left(\vec{\nabla}\phi^{(1)}\right)^2 - \rho\frac{\partial \phi^{(2)}}{\partial t} - \rho\left(\vec{X}^{(1)} \cdot \vec{\nabla}\frac{\partial \phi^{(1)}}{\partial t}\right) \end{aligned} \tag{3.26}$$

The following contributions will lead to second order wave loads:

$$\begin{aligned} \vec{F}_k^{(2)} = &\iint_{S_{k0}} (p^{(1)} \cdot \vec{N}_k^{(1)}) \cdot dS + \iint_{S_{k0}} (p^{(2)} \cdot \vec{n}_k) \cdot dS \\ &+ \iint_{S_k} (p^{(0)} \cdot \vec{N}_k^{(1)}) \cdot dS + \iint_{S_k} (p^{(1)} \cdot \vec{n}_k) \cdot dS \end{aligned} \tag{3.27}$$

The final formulation of the second order wave loads per body is given by:

$$\begin{aligned} \vec{F}_k^{(2)} = &-\rho \iint_{S_{k0}} \left(g\vec{X}_{k3}^{(1)} + \frac{\partial \phi^{(1)}}{\partial t}\right) \cdot \vec{N}_k^{(1)} \cdot dS \\ &-\rho \iint_{S_{k0}} \left(\frac{1}{2}\left(\vec{\nabla}\phi^{(1)}\right)^2 + \vec{X}_k^{(1)} \cdot \vec{\nabla}\frac{\partial \phi^{(1)}}{\partial t}\right) \cdot \vec{n}_k \cdot dS \\ &-\rho \iint_{S_{k0}} \frac{\partial \phi^{(2)}}{\partial t} \cdot \vec{n}_k \cdot dS \\ &-\rho g \iint_{S_k} z \cdot \vec{N}_k^{(1)} \cdot dS \\ &-\rho \iint_{S_k} \left(g\vec{X}_{k3}^{(1)} + \frac{\partial \phi^{(1)}}{\partial t}\right) \cdot \vec{n}_k \cdot dS \end{aligned} \tag{3.28}$$

Again, the second order wave loads can be separated into loads originating from the second order potential and loads originating from the quadratic function of first order terms.

$$\vec{F}_k^{+(2)} = \vec{F}_{pk}^{+(2)} + \vec{F}_{qk}^{+(2)} \tag{3.29}$$

The contribution of the second order potential to the second order wave loads is given by:

$$\vec{F}_{pk}^{+(2)} = \mathrm{i}(\omega_i + \omega_j)\rho \iint_{S_k} (\varphi_I^{+(2)} + \varphi_D^{+(2)}) \cdot \vec{n}_k \cdot dS \tag{3.30}$$

The response due to the second order wave loads is obtained by solving the equation of motion for each frequency pair (ω_i, ω_j):

$$\{-(\omega_i + \omega_j)^2([M] + [A]) - \mathrm{i}(\omega_i + \omega_j)[B] + ([K] + [C])\}\vec{X}^{(2)} = \vec{F}_E^{(2)}(\omega_i, \omega_j) \tag{3.31}$$

where $\vec{X}^{(2)}$ is a vector containing the response of each body in 6 degrees of freedom due to the second order wave loads.

3.2.1. Application to Pioneering Spirit

Both AQWA and Hydrostar are capable of computing the second order wave loads for multiple interacting bodies. In this case AQWA is used to obtain the second order wave loads, for the simple reason that Hydrostar requires an additional license to compute the second order wave loads which was not available at the time of writing this thesis.

A troubling limitation of AQWA is the maximum number of rigid bodies for which the second order wave loads can be calculated. AQWA has a limit of 3 interacting rigid bodies when calculating second order wave loads due to a memory limitation. This would mean that Pioneering Spirit could be divided in a maximum of 3 bodies. The main principal behind the method based on multi-body dynamics is the discretization of an elastic body into a number of rigid bodies. The higher number of discretizations will lead to a more accurate representation of the elastic body.

The second order wave loads can be divided into loads coming from the second order potential and loads coming from the quadratic function of first order terms. These contributions can be identified in the final formulation of the second order wave loads. The first order response of Pioneering Spirit has already been obtained with both methods. The method based on modal decomposition showed that the first order elastic contribution is negligible for wave frequencies up to □ rad/s, which was concluded from the modal amplitudes for the first two structural modes in figures 3.5 and 3.6. This means that for wave frequencies up to □ rad/s the first order hydroelastic response of this vessel doesn't differ that much from its rigid body response.

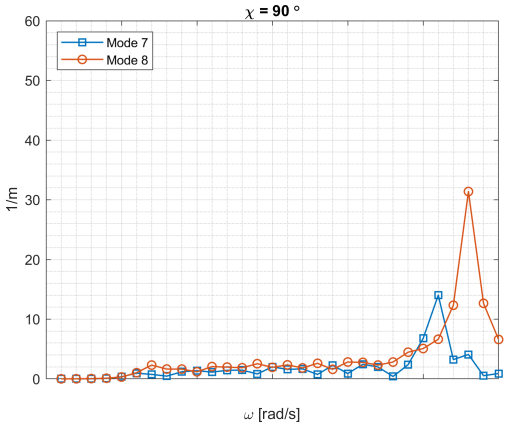

Figure 3.5: RAO mode 7 and 8, $\chi = 90°$

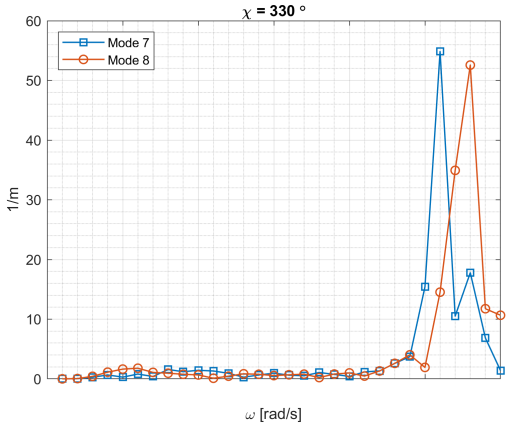

Figure 3.6: RAO mode 7 and 8, $\chi = 330°$

This feature allows to calculate the second order wave loads for each body without exceeding the limit of AQWA. Consider the body indicated with an arrow in figure 3.7. In the left figure the elastic body

is discretized to its desired number of rigid bodies. In the right figure the elastic body is divided into two bodies, the body indicated with an arrow and the remaining bodies modelled as one rigid body. For wave frequencies up to □ rad/s the vessel acts as a rigid body according to the first order theory. This means that the first order hydroelastic response is the same for both discretizations. This also means that the second order wave loads acting on the indicated body are equal for both situations.

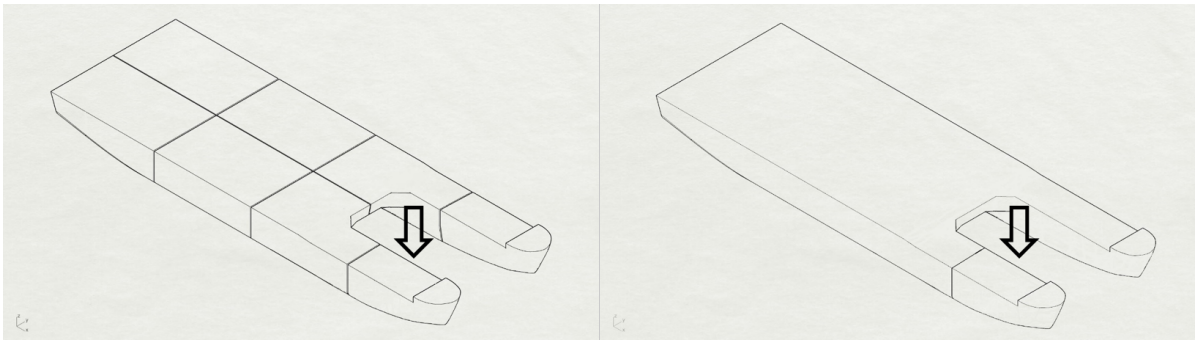

Figure 3.7: Example on how to discretize the vessel

To prove this method a simple test case is constructed. A large floating barge is divided into the maximum allowable bodies in AQWA, which is three (figure 3.9). These bodies are connected to each other with beam elements. The properties of the beam elements are chosen in such a way that the first order hydroelastic response of the elastic barge is equal to its rigid body response up to a certain wave frequency, similar as for Pioneering Spirit. Figure 3.8 shows that for wave frequencies up to 1.1 rad/s the first order response is equal to the rigid body response.

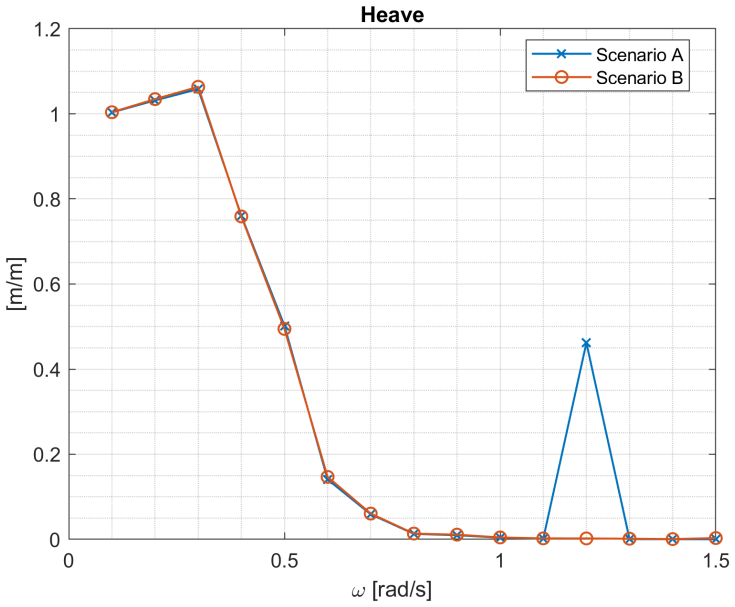

Figure 3.8: Heave RAO for P1 for scenario A and B

Scenario A represents the barge divided into the maximum number of bodies. Scenario B represent the barge divided into two bodies as can be seen in figure 3.9. Since the first order hydroelastic response of both scenario's is equal, the second order wave loads acting on P1 should be equal.

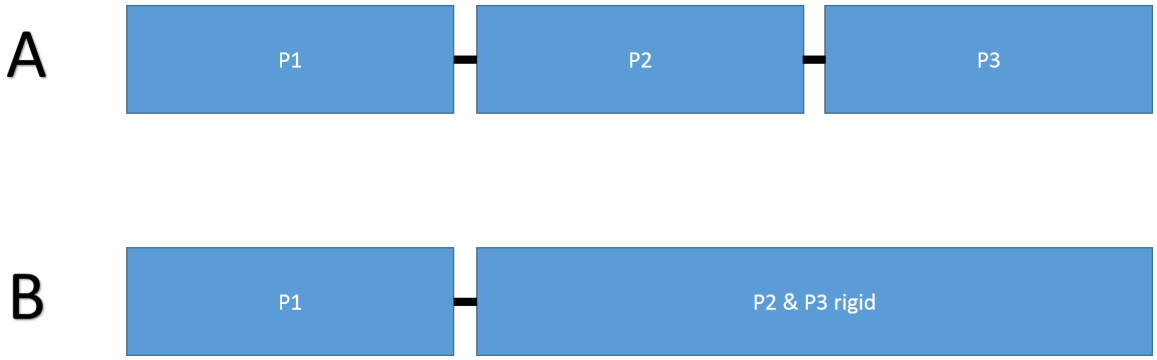

Figure 3.9: Scenario A: Elastic barge divided into 3 bodies
Scenario B: Elastic barge divided into 2 bodies

The second order wave loads acting on P1 are obtained for both scenario's. Figures 3.10 and 3.11 show the quadratic transfer function for the second order wave loads obtained with scenario A and scenario B. It can be seen that scenario B shows very good agreement with scenario A. The second order wave loads are obtained with the same method for P2 and P3, the results are given in figures 3.12 to 3.15. It can be seen that the results from scenario C and D show a good agreement with scenario A as well. This means that as long as the first order hydroelastic response of the elastic body is similar to its rigid body response, the second order wave loads can be obtained with this method.

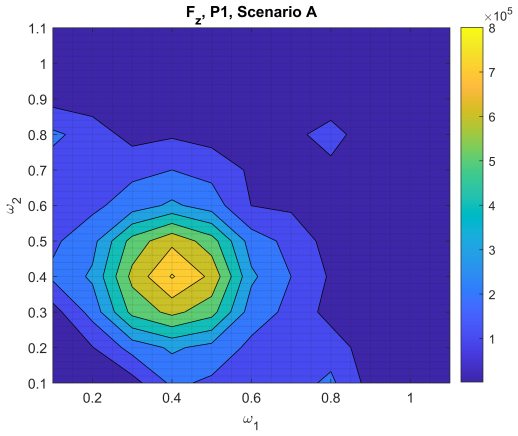

Figure 3.10: QTF for F_z, P1 obtained with scenario A

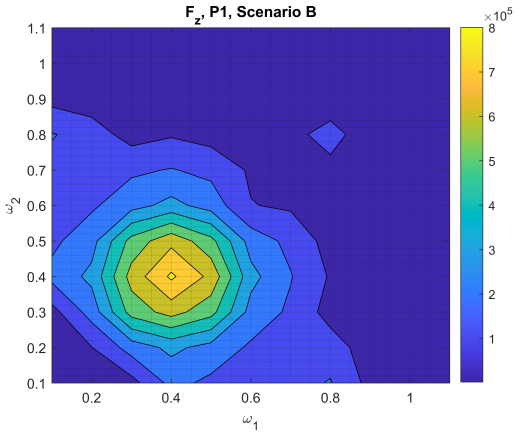

Figure 3.11: QTF for F_z, P1 obtained with scenario B

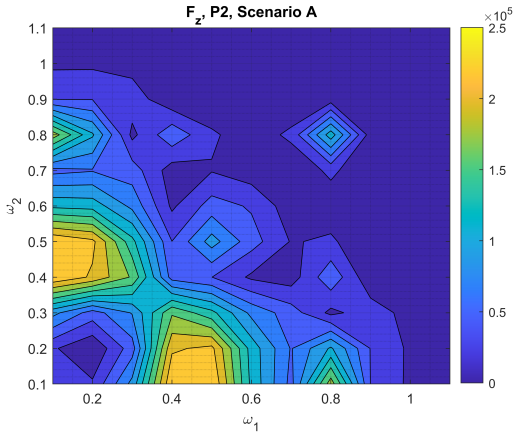

Figure 3.12: QTF for F_z, P2 obtained with scenario A

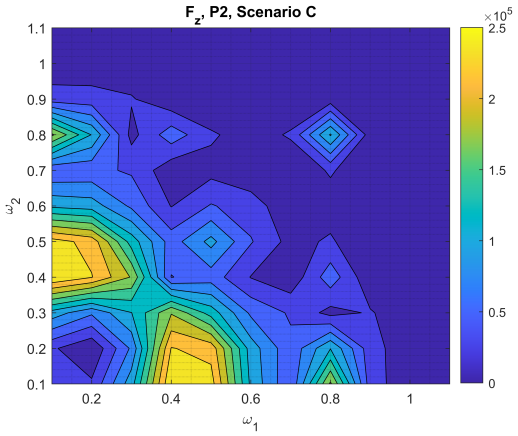

Figure 3.13: QTF for F_z, P2 obtained with scenario C

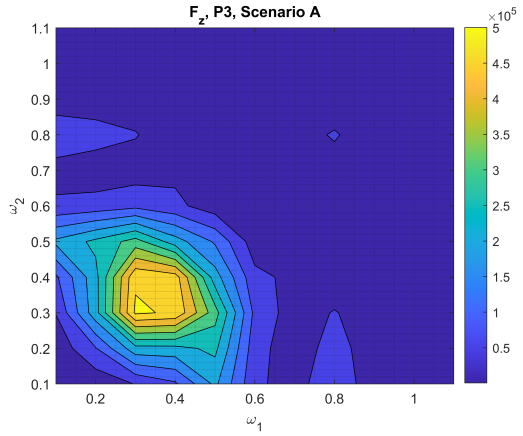

Figure 3.14: QTF for F_z, P3 obtained with scenario A

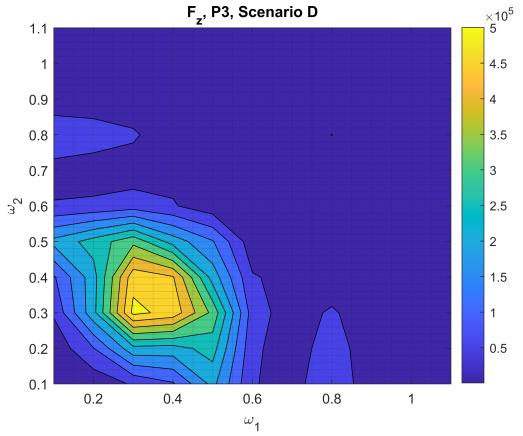

Figure 3.15: QTF for F_z, P3 obtained with scenario D

The second order wave loads are obtained for each body of Pioneering Spirit with the above described method as is shown in figure 3.16. The disadvantage of this method is that a separate analysis has to be performed for each body, which increases the computational time significantly.

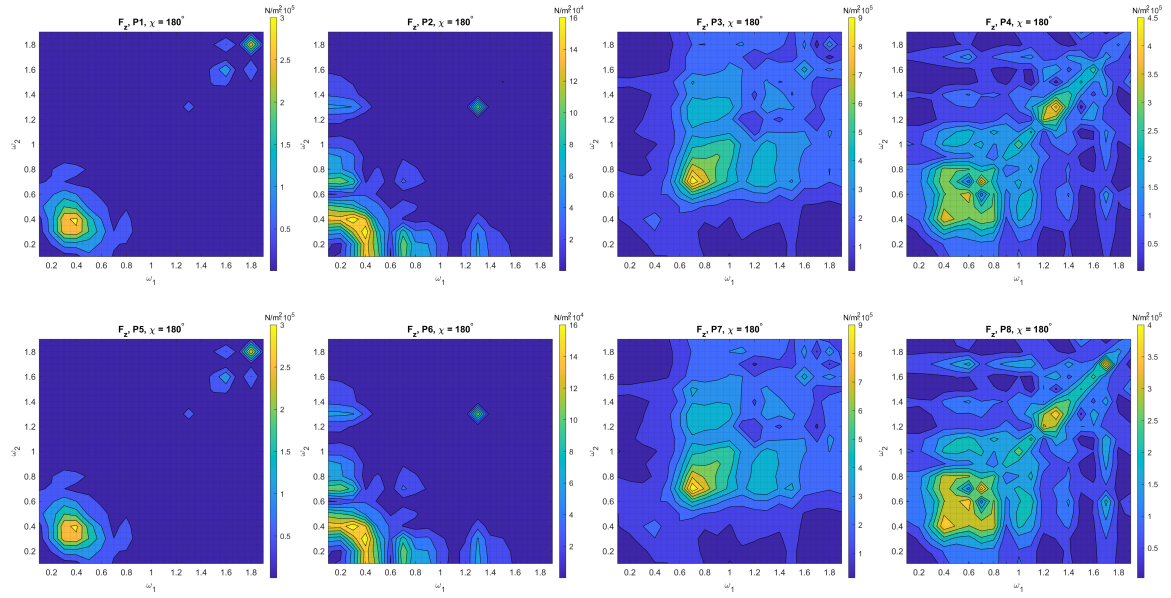

Figure 3.16: $F_z^{+(2)}$ for each body of Pioneering Spirit for an incoming wave direction of $180°$

The main disadvantage of AQWA is that it does not calculate the second order potential. Instead it uses an approximation given by Pinkster [24] to calculate the contribution of the second order potential to the difference-frequency terms of the second order wave loads. For the sum-frequency terms it does not take into account the second order potential at all [1]. This means that the second order wave loads calculated by AQWA only contain $\vec{F}_{qk}^{+(2)}$. Heo & Kashiwagi [12] and Shao & Faltinsen [27] concluded that the contribution of the second order potential is dominant to the sum-frequency terms in the second order wave loads. So, neglecting the contribution of the second order potential will lead to an underestimation of the second order wave loads.

The second order wave loads are substituted into the equation of motion (equation 3.31) to obtain the response of the multi-body model. The response of each rigid body can be transformed to any location on that rigid body with a simple transformation matrix [16]. The second order hydroelastic response is presented in the form of an acceleration spectrum in figure 3.17. It can be seen that the

second order wave loads do cause a certain high-frequent response, but this high-frequent response remains relatively small due to an underestimation of the second order wave loads.

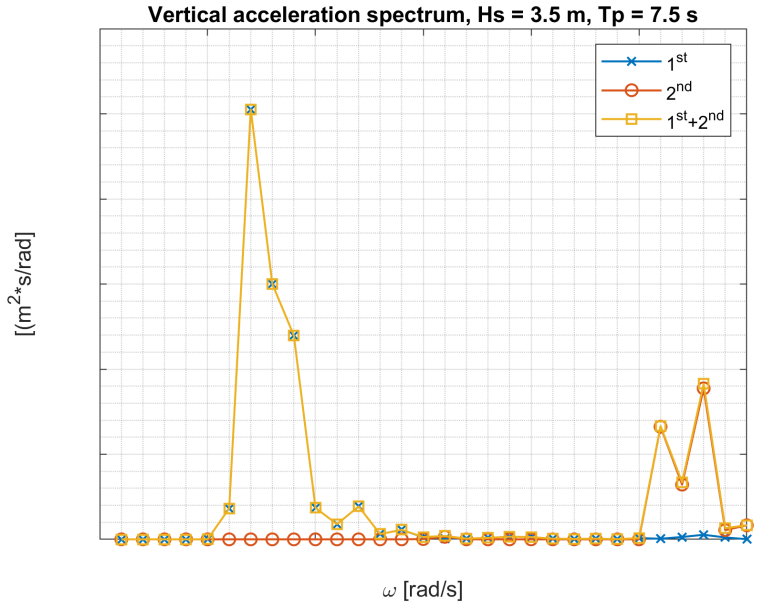

Figure 3.17: Acceleration spectrum containing $\ddot{X}_3^{(1)}$, $\ddot{X}_3^{(2)}$ and $\ddot{X}_3$, obtained with multi-body dynamics

3.3. Summary

This chapter presented the second order theory for both methods and an attempt has been made to apply these methods to Pioneering Spirit to obtain the second order hydroelastic response. The method based on modal decomposition is the most commonly used method to approach hydroelasticity and has been applied to obtain the second order hydroelastic response in a number of studies. However, there is currently no commercial hydrodynamic solver that can obtain the second order hydroelastic response with this method. Therefore, it is yet not possible to predict the second order hydroelastic response with this method.

The method based on multi-body dynamics was proposed as an alternative to eventually overcome this problem. However, the chosen hydrodynamic solver in this method does not calculate the complete second order wave loads. The solver neglects potential part in the sum-frequency terms of the second order wave loads. This contribution is dominant to the sum-frequency terms of the second order wave loads according to Heo & Kashiwagi [12] and Shao & Faltinsen [27]. This is an important difference in the results coming from both methods. In the case of modal decomposition the potential part of the second order wave loads has been taken into account [6, 22], but in the case of multi-body dynamics this part has been neglected [1].

Table 3.1: Equation of motion for both methods

Modal decomposition	$\{-(\omega_i+\omega_j)^2([M]+[A])-\mathrm{i}(\omega_i+\omega_j)[B])+([K]+[C])\}\vec{\zeta}^{(2)}=\vec{F}_p^{+(2)}+\vec{F}_q^{+(2)}$
Multi-body	$\{-(\omega_i+\omega_j)^2([M]+[A])-\mathrm{i}(\omega_i+\omega_j)[B]+([K]+[C])\}\vec{X}^{(2)}=\vec{F}_q^{+(2)}$

4

Results

The first and second order hydroelastic response of Pioneering Spirit is obtained with two different methods. The results coming from these methods are presented in this chapter and are compared to the measured response of Pioneering Spirit. The hydroelastic response of the vessel has been computed for a loading condition with a draft of 11 meters. This condition is chosen, because the second order wave loads based on modal decomposition are provided by Bureau Veritas for this specific draft. However, this isn't a very common draft for the vessel as can be found in appendix B, which means that there is only a small number of measurements that can be used to compare the results to. Measured data from 2016 is used to compute measured response spectra in which a high-frequent response is observed.

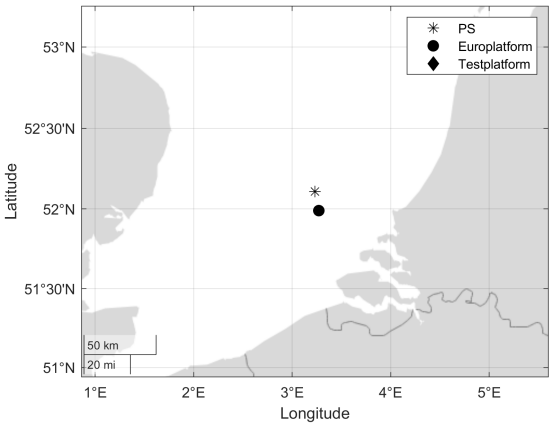

Figure 4.1: Location of vessel, test platform and Europlatform

The directional wave spectra are available for the location of a test platform, see figure 4.1. However, there is a large distance between the vessel and this platform at the time of measurements. Closer located to the vessel is Europlatform. From Europlatform we can get the significant wave height, the mean zero-crossing period and the mean direction of the waves for a certain time interval. This data is used to create a theoretical directional wave spectrum by adopting a Jonswap spectrum with a cosine spreading [11]. The following wave parameters are collected from Europlatform for the intervals A, B and C:

	Part A	**Part B**	**Part C**
$\mathbf{t_{start}}$	16:40	17:40	19:10
$\mathbf{t_{end}}$	17:00	18:10	19:40
$\mathbf{H_s}$	3.5 m	3.2 m	1.5 m
$\mathbf{T_z}$	5.6 sec	5.5 sec	5.2 sec
Mean direction	245°	250°	250°

The wave parameters are used to create a theoretical Jonswap spectrum, $E(\omega)$, and by applying a

cosine-2s spreading a directional wave spectrum can be obtained.

$$
\begin{aligned}
E(\omega,\theta) &= E(\omega)D(\theta) \\
D(\theta) &= A_2 \cos^{2s}(\frac{1}{2}(\theta-\theta_p)) \\
A_2 &= \frac{\gamma(s+1)}{\gamma(s+\frac{1}{2})2\sqrt{\pi}}
\end{aligned}
\tag{4.1}
$$

The spreading parameter s is unknown. According to DNV rules [10] the spreading parameter s is typically between 5 and 15 for wind waves. In this case the spreading parameter s is arbitrarily chosen to be 8.

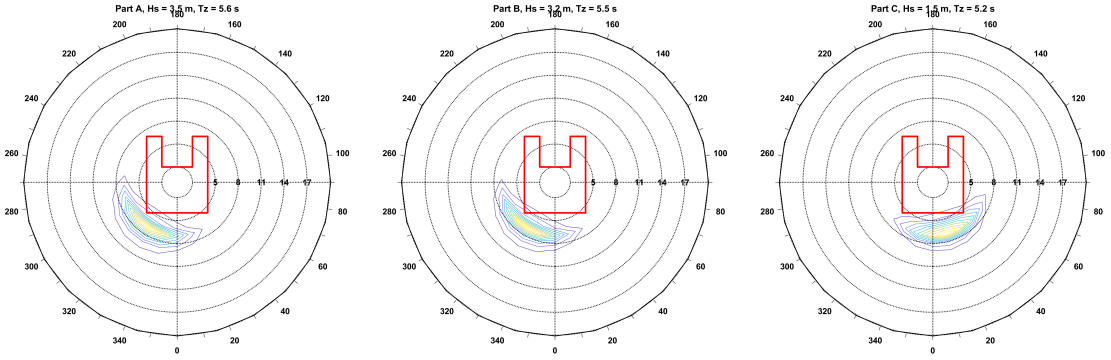

Figure 4.2: Directional wave spectra for each interval

Pioneering Spirit is equipped with a large number of sensors. Four of these sensors are used to measure the response of the vessel at four different locations. These locations are divided over both bows and are denoted as PS AFT, PS FWD, SB AFT and SB FWD (figure 4.3).

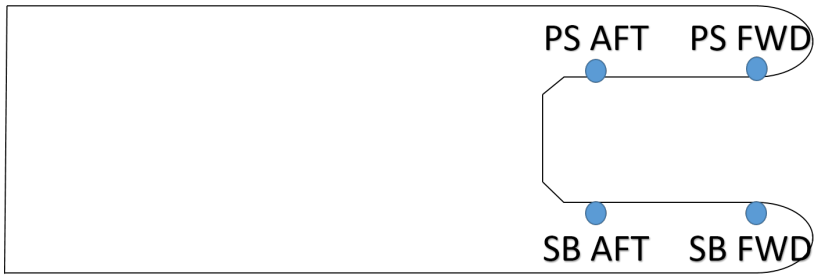

Figure 4.3: Location of the 4 sensors

4.1. Modal decomposition

The method based on modal decomposition is the most commonly used method to approach hydroelasticity. The first and second order hydroelastic response of Pioneering Spirit are obtained with this method and the results are compared to the measured response for intervals A, B and C.

4.1.1. First order response

The first order hydroelastic response is computed with the software package HOMER as is described in chapter 2. The modal amplitudes are calculated for the rigid body modes and a number of structural modes. In the case of Pioneering Spirit the analysis is extended with the first two structural modes.

The modal amplitudes are used to calculate the first order hydroelastic response at locations PS AFT, PS FWD, SB AFT and SB FWD.

Wet natural frequencies
The dry natural frequencies of the vessel consider the structural mass and structural stiffness of the vessel. The presence of water adds mass, damping and stiffness to the dynamics of the vessel. Taking into account the added mass and hydrostatic stiffness of the vessel results in wet natural frequencies. The frequency domain identification technique described in [5] is used to obtain the wet natural frequencies from the measured time series. These wet natural frequencies are compared to the natural frequencies computed by HOMER. These results are given in table 4.1.

Table 4.1: Wet natural frequencies: Operational Modal Analysis vs Modal decomposition

	OMA	Modal decomposition	error %
Mode 7	☐ Hz	☐ Hz	0.48
Mode 8	☐ Hz	☐ Hz	4.44

The wet natural frequencies obtained with the method based on modal decomposition show good agreement with the measured wet natural frequencies. The natural frequency of mode 8 is predicted a bit higher than the measured natural frequency, but within a reasonable range. More interesting is the fact that the wet natural frequencies of both modes are really close to each other, whereas the dry natural frequencies are further away from each other.

The vertical acceleration spectra considering first order wave loads are obtained for each location and each interval. Figure 4.4 shows results for modal decomposition and the measured vertical acceleration spectra for part A. The first order theory shows very good agreement with the wave-frequent part, but as expected the first order theory shows no response at the high-frequent part. There is almost no wave energy present around these high frequencies in the wave spectrum, resulting in a negligible response at these frequencies.

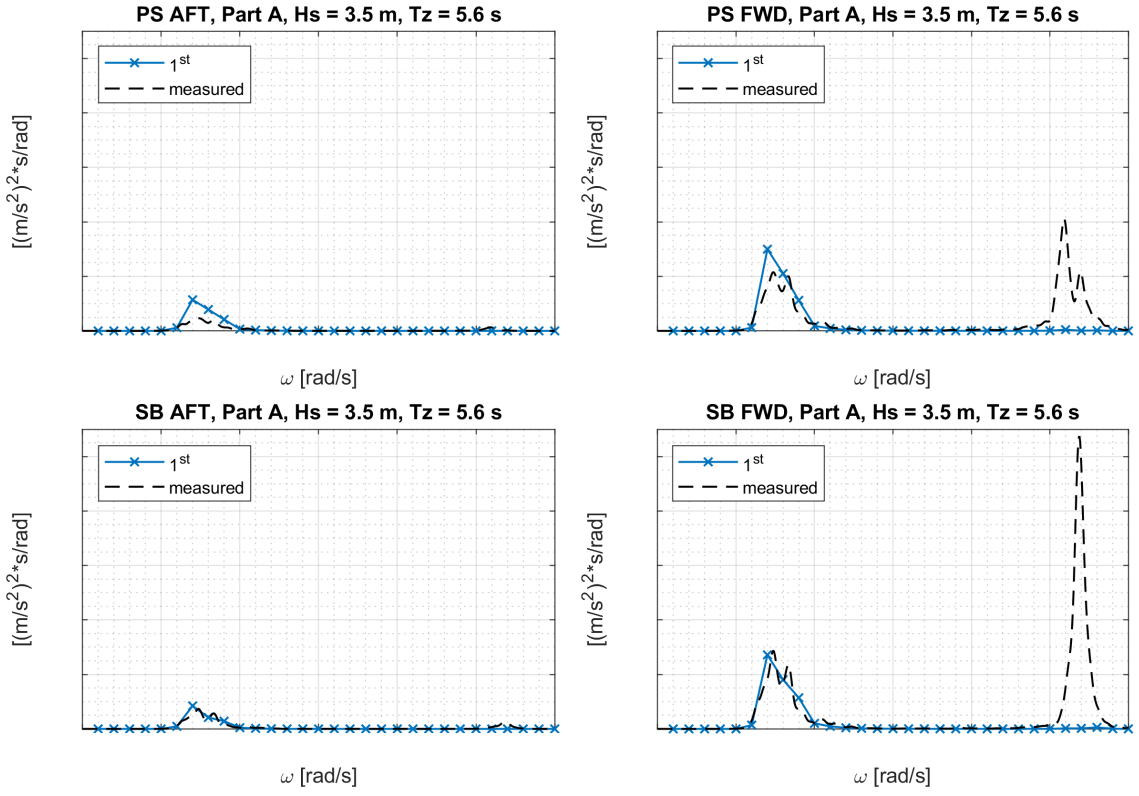

Figure 4.4: Vertical acceleration spectra considering first order wave loads for part A

4.1.2. Second order response

The second order hydroelastic theory is explained in chapter 3. The second order theory allows to calculate wave loads at higher frequencies than the encountered wave frequencies and have the possibility to excite the natural modes of the vessel.

Figures 4.5, 4.6 and 4.7 show the second order hydroelastic response for each interval and location. It can be seen that the results obtained with modal decomposition show good agreement with the measured response of the vessel. The fact that the wave-frequent part shows good agreement as well creates confidence that the wave spectra are determined accurately enough.
The highest accelerations are measured at starboard. These large peaks are caused by excitation of the second structural mode. This can also be seen in the structural modes coming from the finite element model. The second modeshape shows a higher value at starboard. It can be seen that the magnitude of the response is well predicted by the method based on modal decomposition, but it predicts the response at a higher frequency. It was already shown in table 4.1 that the wet natural frequency of the second structural mode tends to be overpredicted.
The high-frequent response decreases significantly for interval C, compared to interval A and B. This decrease is also predicted by the method based on modal decomposition. It seems that this decrease in high-frequent response is mainly caused by the decrease in significant wave height.

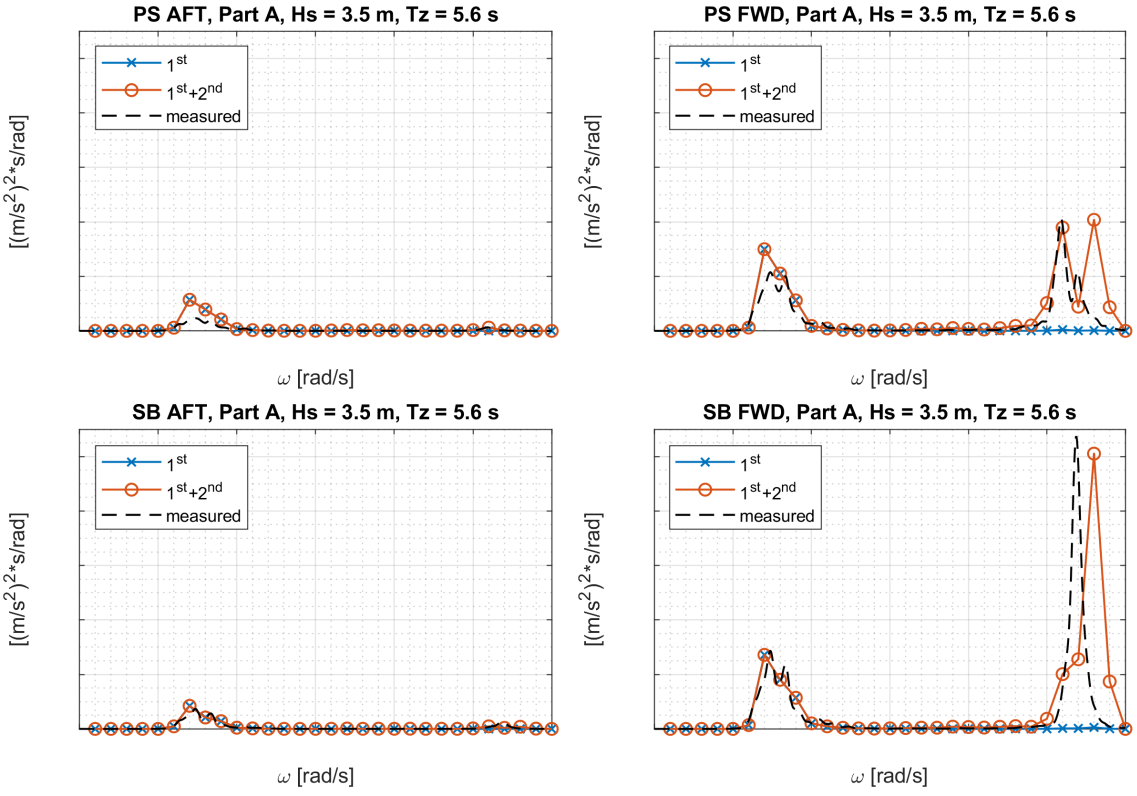

Figure 4.5: Second order hydroelastic response obtained with modal decomposition for part A

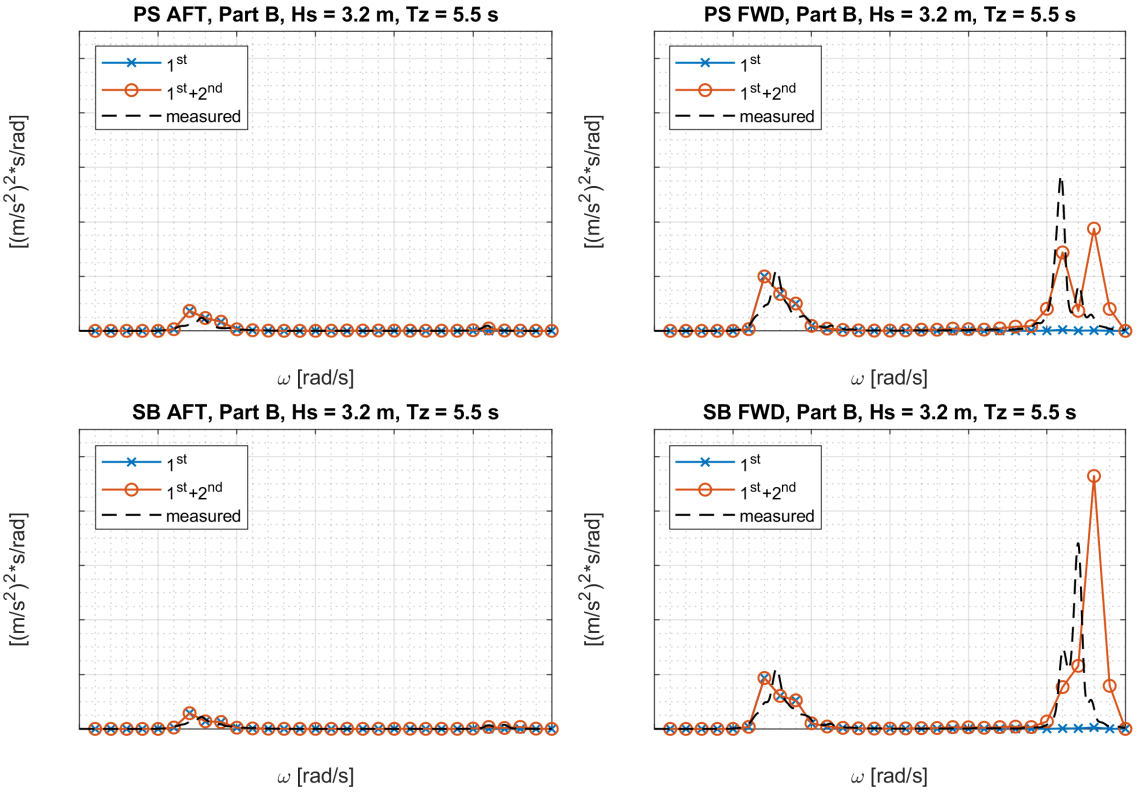

Figure 4.6: Second order hydroelastic response obtained with modal decomposition for part B

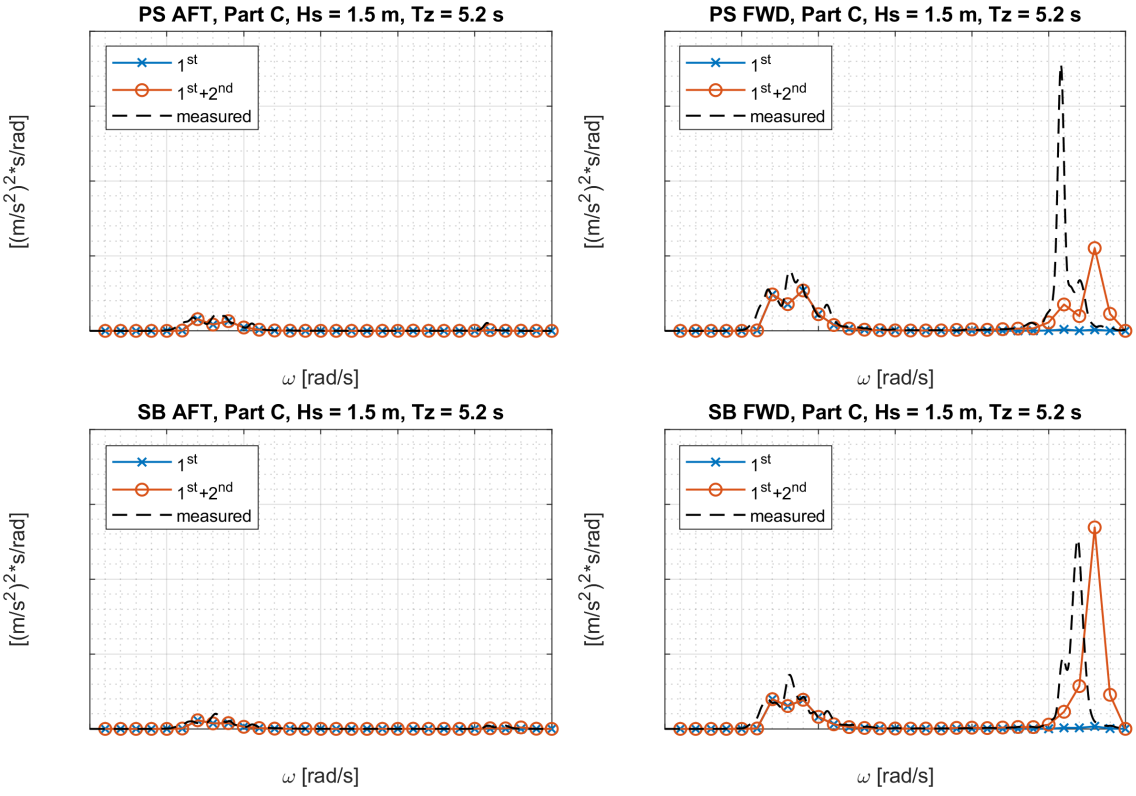

Figure 4.7: Second order hydroelastic response obtained with modal decomposition for part C

4.2. Modal decomposition vs Multi-body dynamics

It is shown that second order wave loads have a major contribution to the high-frequent response of the vessel. The method based on multi-body dynamics is proposed as an alternative method to approach hydroelasticity. In this section the hydroelastic response obtained with multi-body dynamics will be compared to the hydroelastic response obtained with modal decomposition.

4.2.1. First order response

The first order hydroelastic response coming from multi-body dynamics will be compared to the results from modal decomposition to test wether the multi-body is accurate enough to capture the hydroelastic response.

Wet natural frequencies

The wet natural frequencies from the multi-body model are compared to the wet natural frequencies obtained with modal decomposition. It can be seen that the multi-body model overestimates the wet natural frequencies for both structural modes. The multi-body model has been tuned to match the dry natural frequencies and modeshapes coming from the finite element model. These modeshapes from the finite element model also form the basis for the method based on modal decomposition. The dry natural frequencies have an error of less than one percent as can be seen in table 2.2 in chapter 2, but the wet natural frequencies have a larger error.

Table 4.2: Wet natural frequencies: Modal decomposition & Multi-body

	Modal decomposition	**Multi-body**	**error %**
Mode 7	□ Hz	□ Hz	4.83
Mode 8	□ Hz	□ Hz	1.56

The response amplitude operators are obtained for each body within the multi-body model. Since it is assumed that each body acts as a rigid body, the response at any location on that body can be calculated with a simple transformation matrix.
Figures 4.8 to 4.11 show the response amplitude operators for location PS FWD for a number of incoming wave directions. These figures also show the response amplitude operators that are obtained with the method based on modal decomposition. In most cases the wave frequent part matches very well, but in some cases some larger discrepancies appear in the wave-frequent part as can be seen for example in figure 4.11.
The wet natural frequencies are being overestimated, but the amplitudes of the high-frequent response show very good agreement with the amplitudes obtained with modal decomposition. Next to that, the multi-body model also matches the type of structural mode that is being excited. For example, for an incoming wave direction of 0° it is the second structural mode, so vertical bending, that is being excited according to modal decomposition and this second structural mode is also excited in the multi-body model. Except for the wet natural frequencies, the results show very good agreement with the results obtained with modal decomposition.

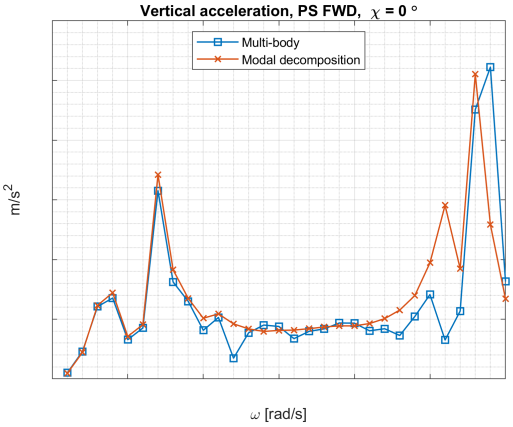

Figure 4.8: $\chi = 0°$

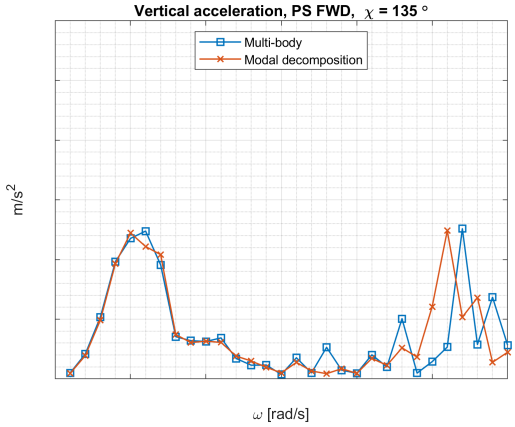

Figure 4.9: $\chi = 135°$

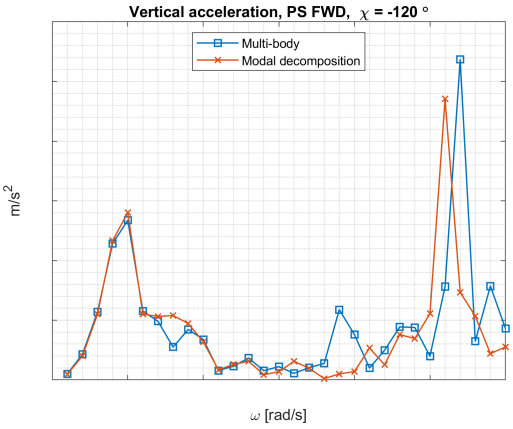

Figure 4.10: $\chi = -120°$

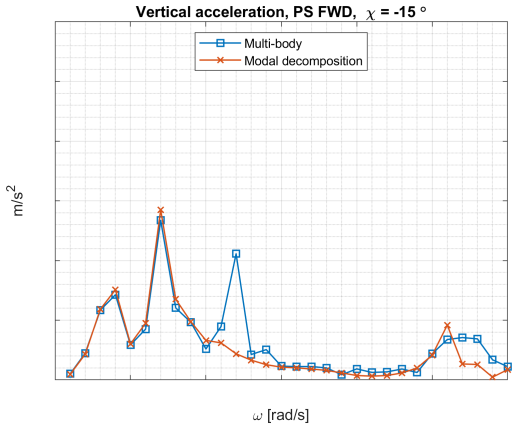

Figure 4.11: $\chi = -15°$

4.2.2. Second order response

The second order hydroelastic response is obtained with the multi-body model. This second order hydroelastic response is presented in the form of an acceleration spectrum. Figures 4.12 and 4.13 show acceleration spectra obtained with both methods. It can be seen that the method based on multi-body dynamics shows a significant lower high-frequent response than the method based on modal decomposition. This is most likely due to the fact that the second order wave loads have been underestimated in the case of multi-body dynamics. The multi-body analysis has only taken into account the quadratic part of the second order wave loads, whereas the modal decomposition analysis has taken into account both the quadratic an the potential part of the second order wave loads. According to a number of studies [12, 27], the potential part has a dominant contribution to the sum-frequency terms of the second order wave loads and can not be neglected when calculating the second order hydroelastic response.

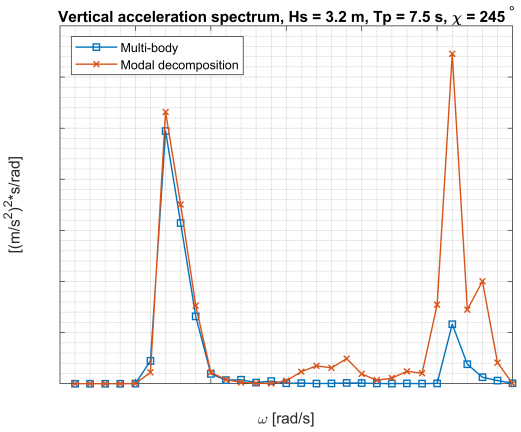

Figure 4.12: $\chi = 245°$

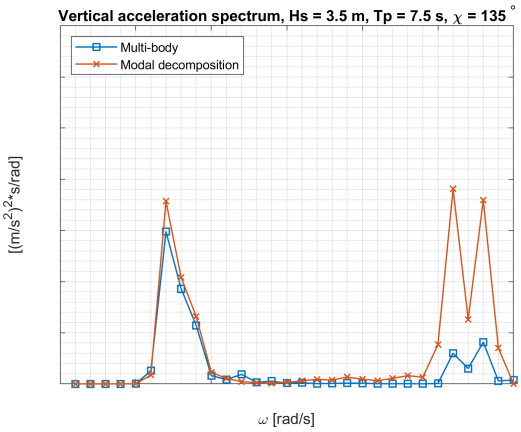

Figure 4.13: $\chi = 135°$

The wave conditions from interval A, B and C are used to create acceleration spectra with the multi-body model. These spectra are compared to the acceleration spectra obtained with modal decomposition and the measured acceleration spectra. The results are shown in figures 4.14, 4.15 and 4.16. The results obtained with multi-body dynamics show little resemblance with the measured response. The method predicts that there is a certain high-frequent response for each interval, but underestimates this high-frequent response significantly. It is expected that a better agreement can be found when the complete second order wave loads are taken into account in the case of multi-body dynamics.

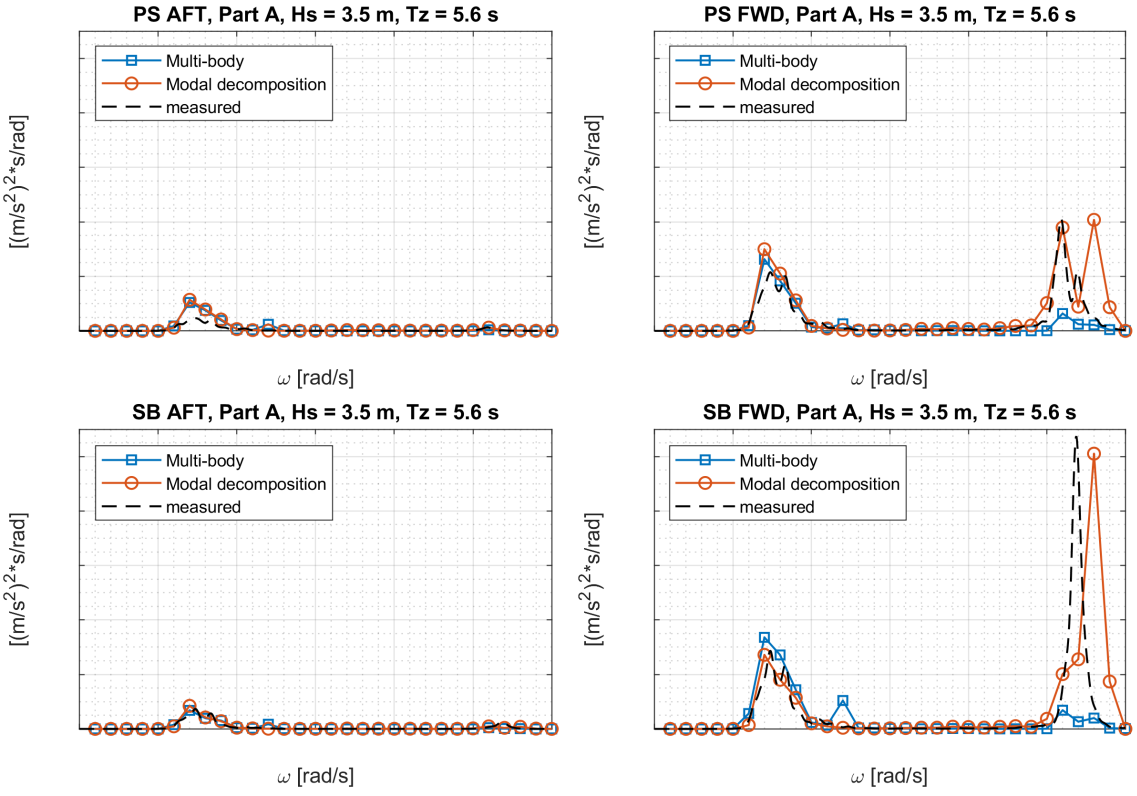

Figure 4.14: Hydroelastic response taking into account second order wave loads, part A

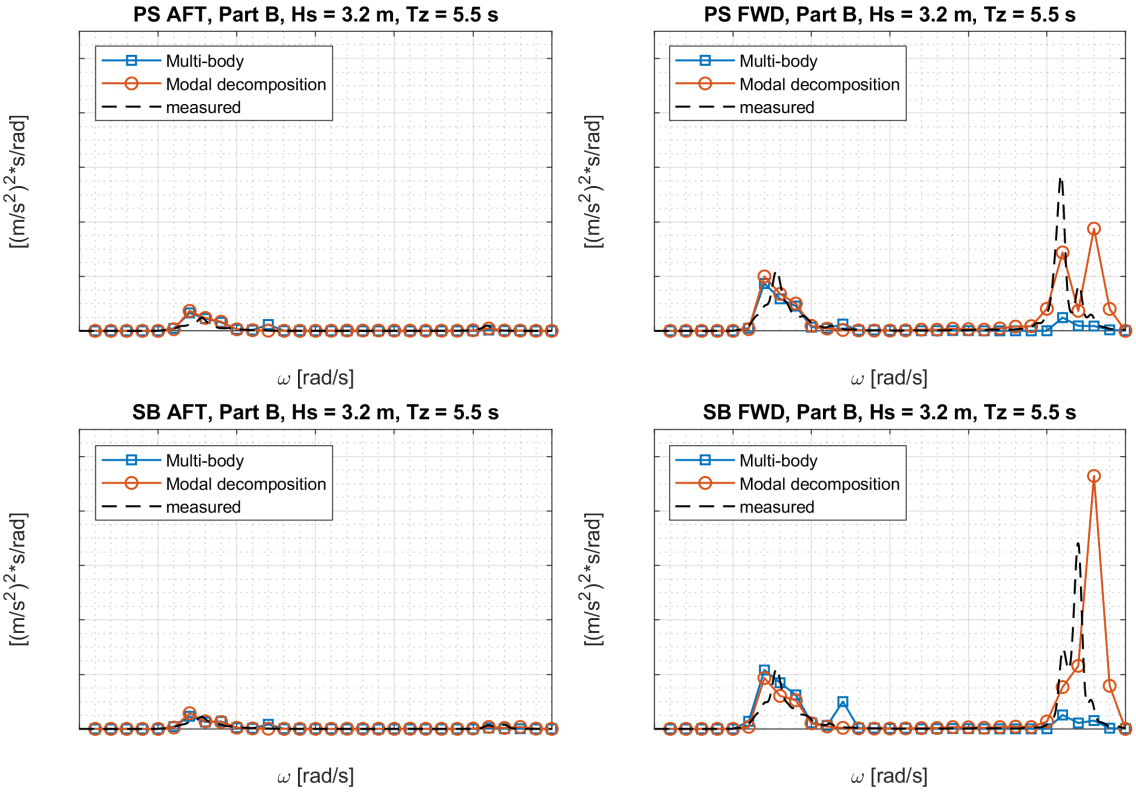

Figure 4.15: Hydroelastic response taking into account second order wave loads, part B

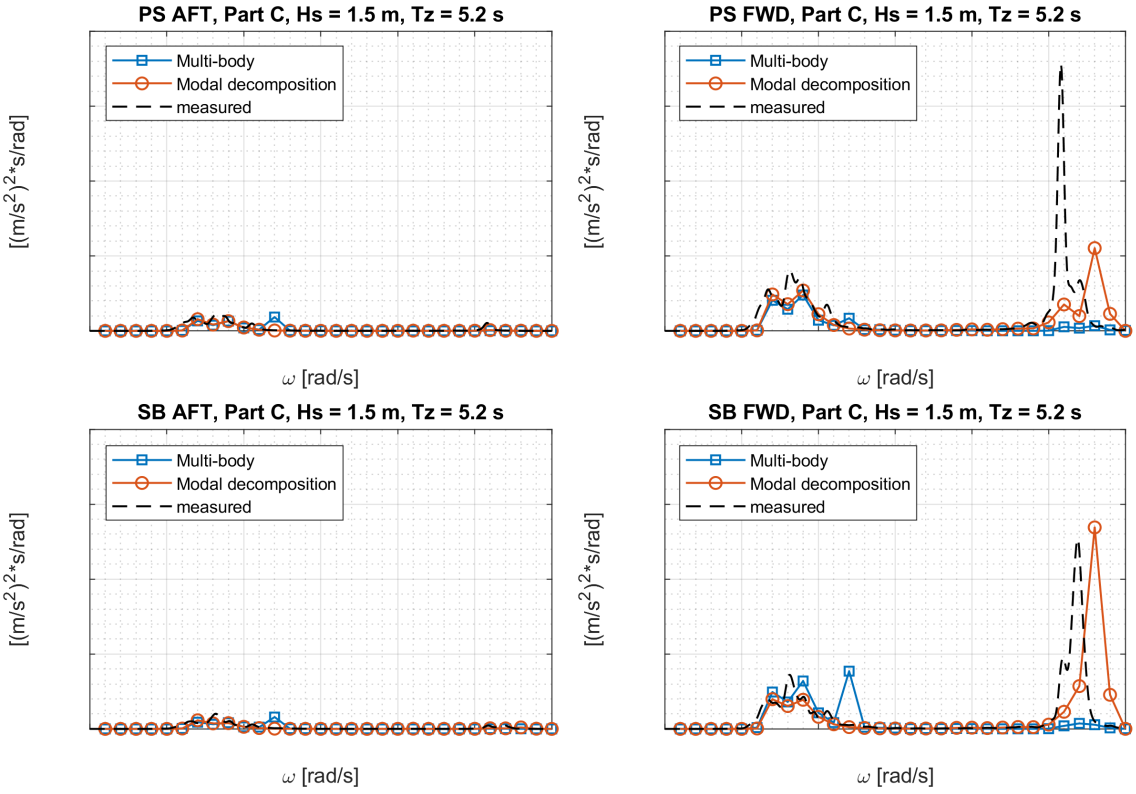

Figure 4.16: Hydroelastic response taking into account second order wave loads, part C

5

Sensitivity study

The hydroelastic response obtained with the method based on modal decomposition showed good agreement with the measured response as was shown in chapter 4. The results are obtained with a theoretical wave spectrum from which the wave parameters are based on measurements from a location nearby. The exact environmental conditions at the location of the vessel and time of measurements are unknown. This chapter will present the results from a sensitivity study, in which the sensitivity of the predicted response, based on modal decomposition, to the environmental conditions is tested. The sensitivity to wave spreading and incoming wave directions is tested.

5.1. Wave spreading

The wave parameters used in chapter 4 are based on measurements from a location nearby, except the wave spreading parameter. This parameter is based on DNV rules [10]. According to DNV this spreading parameter is typically between 5 and 15. The response is predicted with different spreading parameters to test the sensitivity to this parameter. Figure 5.1 shows the response for a range of wave spreading parameters varying between 5 and 15. It can be seen that the spreading parameter influences the wave-frequent part of the response a lot more than the high-frequent part of the response.

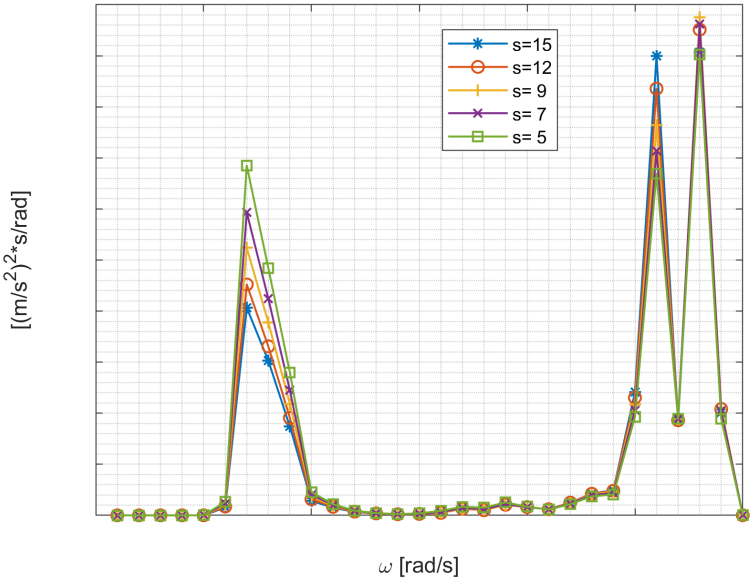

Figure 5.1: Vertical acceleration spectra with varying wave spreading parameter s

5.2. Incoming wave direction

The next parameter that will be tested is the incoming wave direction. The second order hydroelastic response is obtained for incoming wave directions varying from $0°$ to $360°$ to identify which incoming wave directions will cause higher responses. Figures 5.2 shows the results for the locations PS FWD and SB FWD. It can be seen that $0°$, $135°$, $180°$ and $225°$ will lead to a significant high-frequent response. Incoming wave directions of $135°$ and $225°$, so bow quartering waves, will excite the first structural mode. Incoming wave directions of $0°$ and $180°$ will excite the second structural mode.

More interesting to see are the directions in which a respectively low response would have been expected. It can be seen that for incoming wave directions of $50°$ and $310°$ the response appears to be quite low. These waves can be classified as stern quartering waves. The vessel actually experienced these stern quartering waves during the considered intervals in chapter 4. According to figure 5.2 the high-frequent response could have been a lot higher if the heading of the vessel would have been different.

This figure also shows that at portside the hydroelastic response mainly comes from excitation of the first structural mode, whereas at starboard the hydroelastic response mainly comes from the second structural mode, which was also seen in the measured response.

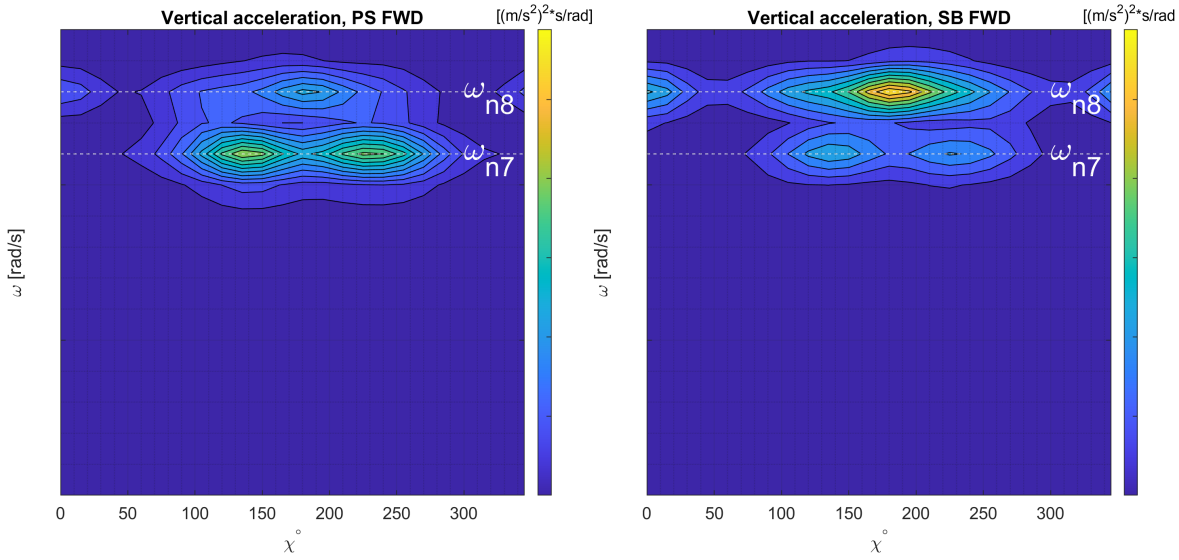

Figure 5.2: Acceleration spectrum for incoming wave directions from $0°$ to $360°$

6

Discussion

This chapter will discuss the results that are presented in chapter 4 and take a critical look at the methods that are used to obtain these results. Next, this chapter reviews the hypotheses that are formulated in chapter 1 to decide whether these hypotheses can be accepted or rejected.

6.1. Modal decomposition

The first method that is discussed is the method based on modal decomposition. The first and second order hydroelastic response were presented and it was shown that the second order wave loads have a large contribution to the total hydroelastic response. A good agreement was found between the measured response and the predicted response taking into account these second order wave loads. However, some points need to be addressed regarding the results.

6.1.1. Wave spectrum

The predicted hydroelastic response was compared to the measured response by comparing the measured and predicted acceleration spectra. These spectra were computed using theoretical wave spectra, because there was no measured wave spectrum available at the location of the vessel at the time of measurements. The used wave parameters were measured at a distance of approximately 13 km from Pioneering Spirit. The wave spreading parameter was chosen arbitrarily, but based on DNV rules. It was shown in chapter 5 that this wave spreading parameter does not have a large influence on the prediction of the high-frequent response. The wave-frequent is more sensitive to the wave spreading parameter. The wave spreading parameter has been tuned to match the wave frequent part of the predicted response with the measured response. A better approximation of the directional wave spectra could be made with SWAN [4], which is a numerical wave model developed at TU Delft.

6.1.2. Small number of measurements

The second order hydroelastic response has only be obtained for Pioneering Spirit with a draft of 11 meter. This is because the second order wave loads were provided by Bureau Veritas for this specific draft. However, this draft is not a common draft for Pioneering Spirit, which has led to only a small number of measurements to compare the second order hydroelastic response to.

6.1.3. First hypothesis

The second order hydroelastic response is obtained with the method based on modal decomposition to test the first hypothesis:

The observed high-frequent response of Pioneering Spirit is caused by second order wave loads.

The hydroelastic response has been obtained for three different wave spectra. In all these three wave spectra there is little to no wave energy around the natural frequencies of the vessel, leading to a

negligible first order hydroelastic response. Taking into account the second order wave loads has led to a significant increase in the hydroelastic response around these natural frequencies. The second order hydroelastic response is compared to full-scale measurements and a very good agreement was found. From the results it can be concluded that the observed high-frequent response of Pioneering Spirit is indeed caused by second order wave loads.

6.2. Multi-body dynamics

The method based on multi-body dynamics has been proposed as an alternative method to approach hydroelasticity for Pioneering Spirit. Although the method based on modal decomposition showed very good results, it has the main disadvantage that the second order hydroelastic response cannot be obtained with commercial software yet. The first and second order hydroelastic response have been obtained with the method based on multi-body dynamics. The response amplitude operators obtained with multi-body dynamics are compared to the response amplitude operators obtained with modal decomposition in chapter 4. The wet natural frequencies are overestimated with the multi-body model, but the amplitudes of the linear transfer functions (RAO's) show very good agreement with the ones obtained with modal decomposition.

6.2.1. Reduced stiffness matrix

The multi-body model is far from ideal. A very simple reduced order model has been made by simplifying the vessel to a small number of lumped masses connected to each other with beam elements. The reduced order model should approximate the actual mass and stiffness of the vessel. The most accurate representation is given by a finite element model of the vessel. The beam elements of the beam model have been tuned to match the first two dry natural frequencies and modeshapes of the finite element model. This is a very simplified approach to approximate the structural behaviour of a complex structure as Pioneering Spirit. Within the field of structural dynamics, more sophisticated model reduction techniques exist. Adopting one of these techniques could lead to better reduced order model considering the structural dynamics. Nevertheless, the beam model still showed good correlation with the finite element model considering the first two structural modes.

6.2.2. Mesh size

The multi-body model overestimates the wet natural frequencies compared to the method based on modal decomposition. In both methods the hydrodynamic terms are solved with the same hydrodynamic solver: Hydrostar. Both models have a similar mesh size and contain around 15,000 diffracting elements. However, the multi-body model also contains elements between subsequent bodies as can be seen in figure 6.1. Both models have a similar number of elements, but the multi-body model contains less elements at the outer hull. It has been checked that the hydrodynamic analysis remains stable at the higher wave frequencies, but no proper mesh convergence study has been performed. A larger mesh size could lead to more accurate results for the hydrodynamic terms at these higher frequencies.

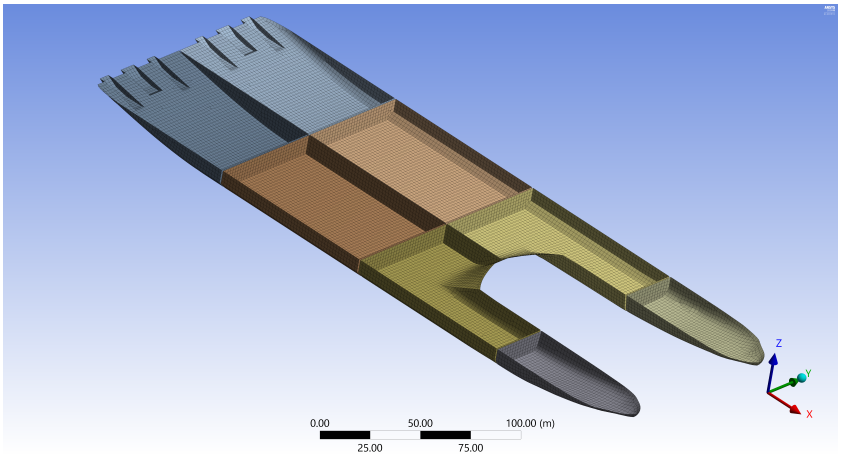

Figure 6.1: Mesh contains elements between subsequent bodies

6.2.3. Discretization

The elastic body is discretized into a number of rigid bodies. A higher number of bodies leads to a more accurate representation of the elastic body. Pioneering Spirit is divided into a quite small number of bodies to eventually reduce the computational time. That is because each body required a separate analysis to obtain the second order wave loads. It was found that the dry modeshapes could be reproduced with this limited amount of bodies. A larger number of bodies could in this case lead to more accurate results. Besides that, one could argue if this partition of bodies is the most optimal. When discretizing an elastic body into rigid bodies, the body is divided in a certain dimension because it is expected that the body does deform along that dimension. A quick look at the modeshapes indicates that Pioneering Spirit mainly deforms along the length of the vessel. Even in the case of torsion, the main direction in which deformation occurs is along the length of the vessel. Therefore, it would be much more efficient to divide the vessel over its length.

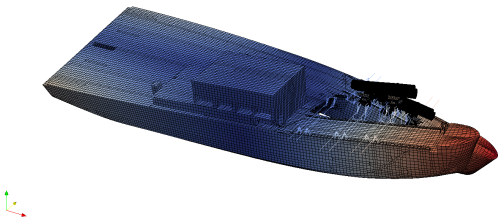

Figure 6.2: FEM mode 7, $f_n = \square Hz$

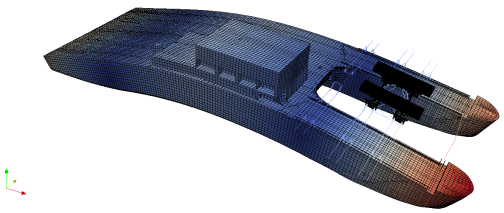

Figure 6.3: FEM mode 8, $f_n = \square Hz$

The multi-body model of Pioneering Spirit could be improved a lot. The first order hydroelastic response already shows good agreement with the results coming from the method based on modal decomposition. It is expected that improving the multi-body model on the mentioned points will result in a better agreement between both methods considering the first order hydroelastic response.

6.2.4. Second order potential

The second order wave loads were obtained with AQWA. It can be stated that AQWA is not the ideal hydrodynamic solver to obtain second order wave loads on an elastic body. The first problem that was encountered was the maximum number of bodies to calculate second order wave loads, due to a memory limit of the software. This is a major disadvantage in the case of a multi-body model. However, due to the negligible first order hydroelastic response of Pioneering Spirit, a method could be proposed to work around this limit.

The main disadvantage of AQWA is that it does not calculate the second order potential. It uses an approximation from Pinkster [24] to approximate the potential part of the difference-frequency terms of

the second order wave loads, but for the sum-frequency terms it neglects the potential part completely [1]. AQWA only calculates the second order wave loads that originate from first order terms $\vec{F}_{qk}^{+(2)}$.

$$\vec{F}_k^{+(2)} = \vec{F}_{pk}^{+(2)} + \vec{F}_{qk}^{+(2)} \tag{6.1}$$

The potential part $\vec{F}_{pk}^{+(2)}$ has a dominant contribution to the sum-frequency terms of the second order wave loads according to Heo & Kashiwagi [12] and Shao & Faltinsen [27]. It is most likely that the obtained second order wave loads are being underestimated. This could explain the very poor agreement with the method based on modal decomposition considering the second order hydroelastic response, because the potential part has been taken into account in the second order wave loads for modal decomposition [6, 22].
This doesn't mean that the multi-body model is not able to obtain the second order hydroelastic response. The current multi-body model obtains the second order hydroelastic response, but only for a part of the second order wave loads. It is recommended to use a different hydrodynamic solver that does calculate the second order potential for the sum-frequency terms. For example, the hydrodynamic solver Hydrostar. This solver is able to calculate second order wave loads in a multi-body analysis and does calculate the second order potential [6]. It is expected that a better agreement can be found when the complete second order wave loads are being taken into account for the multi-body model.

6.2.5. Second hypothesis

The method based on multi-body dynamics has been proposed as an alternative to approach hydroelasticity for Pioneering Spirit, especially to obtain the second order hydroelastic response. The second hypothesis that was formulated in chapter 1 is:

The second order hydroelastic response of Pioneering Spirit can be approached using multi-body dynamics.

The linear transfer functions (RAO's) showed good agreement with the method based on modal decomposition, but still shows some discrepancies. The multi-body model can be improved on a number of points to improve the agreement between both methods.
At this moment it can not be said if the second order hydroelastic response can be predicted with multi-body dynamics as well. An important part of the second order wave loads is missing in the second order hydroelastic response, resulting in little resemblance with the method based on modal decomposition and with the full-scale measurements.

7

Conclusion & Recommendations

The first objective of this thesis was to find an explanation for the observed high-frequent response of Pioneering Spirit by considering the vessel as an elastic body. This research objective has been reached by approaching the hydroelastic behaviour of the vessel with modal decomposition. Considering second order wave loads in this method resulted in a significant increase of the response around the natural frequencies compared to the first order hydroelastic response. The results were compared to the full-scale measurement of the vessel and showed very good agreement. It is concluded that second order wave loads cause the high-frequent response of the vessel.

The method based on modal decomposition is considered to be a reliable method to predict the first and second order hydroelastic response of the vessel. Most of the studies regarding hydroelasticity also rely on this method to approach hydroelasticity of ships. Another method that could be used to approach hydroelasticity is the method based on multi-body dynamics. So far, this method has most commonly been used to approach hydroelasticity for Very Large Floating Structures. In this thesis this method has been proposed as an alternative method to approach hydroelasticity of a large vessel as Pioneering Spirit. An important reason to propose a different method is the fact that at this moment no commercial software is able to calculate the second order hydroelastic response with the method based on modal decomposition.

The second objective was to create a multi-body model of Pioneering Spirit that can predict the high-frequent response of the vessel. It was shown that the observed high-frequent response is caused by second ware loads, so the multi-body model should eventually calculate the second order hydroelastic response.

First, the RAO's from the multi-body model were compared to the RAO's obtained with modal decomposition to verify that the multi-body model is able to approach the hydroelasticity of the vessel. The amplitudes of the RAO's showed good agreement with the ones obtained with modal decomposition. The multi-body model is able to capture the excitation of the corresponding natural mode, but slightly overestimates the wet natural frequencies. Overall, the multi-body model showed very good results given the simplicity of the current multi-body model.

The second order wave loads were obtained for the multi-body model to eventually obtain the second order hydroelastic response of Pioneering Spirit. The second order wave loads were obtained with AQWA. This hydrodynamic solver doesn't take into account the second order potential for the sum-frequency terms of second order wave loads [1]. In the method based on modal decomposition the second order potential has been taken into account [6, 22]. Comparing the results from both methods showed that the second order hydroelastic response was underestimated significantly in the case of multi-body dynamics. It is most likely that this underestimation of the response is caused by an underestimation of the second order wave loads. A number of studies have shown that the second order potential has a large contribution to the sum-frequent terms of the second order wave loads. The second order potential can simply not be neglected in the second order hydroelastic response [12, 27].

Altogether, it can be concluded that the observed high-frequent response of Pioneering Spirit is caused by second order wave loads and that the multi-body model is yet not able to predict this high-frequent response. However, it has been shown that the hydroelastic behaviour of a complex structure as Pioneering Spirit can be modelled with a relatively simple multi-body model and it is believed that taking into account the second order potential in the second order wave loads will lead to a more accurate approximation of the high-frequent response with this multi-body model.

7.1. Recommendations

It is concluded that the results obtained with modal decomposition show good agreement with the measured response. The agreement between the numerical results and measurements could be improved by a better approximation of the encountered wave spectra. There is a small overestimation of the wet natural frequency of the second structural mode, which could be improved as well.

The main recommendation is to improve the multi-body model, because the method based on multi-body dynamics has the potential to predict the high-frequent response of Pioneering Spirit in the future. It is recommended to improve the multi-body model on the following points:

1. The elastic body is discretized into a number of rigid bodies. A higher number of bodies will give a better approximation of the behaviour of the elastic body. It is recommended to increase the amount of bodies.
   Extra attention should be paid on how the elastic body is divided into multiple rigid bodies. As discussed in chapter 6, the elastic body is divided along a certain dimension because it is expected that the elastic body does deform along that dimension. It is known that for the first two structural modes the vessel mainly deforms along its length. In terms of efficiency, it is recommended to add more partitions along the length of the vessel instead of the width of the vessel. An example on how the partition of the multi-body model could be improved is given in figure 7.1.

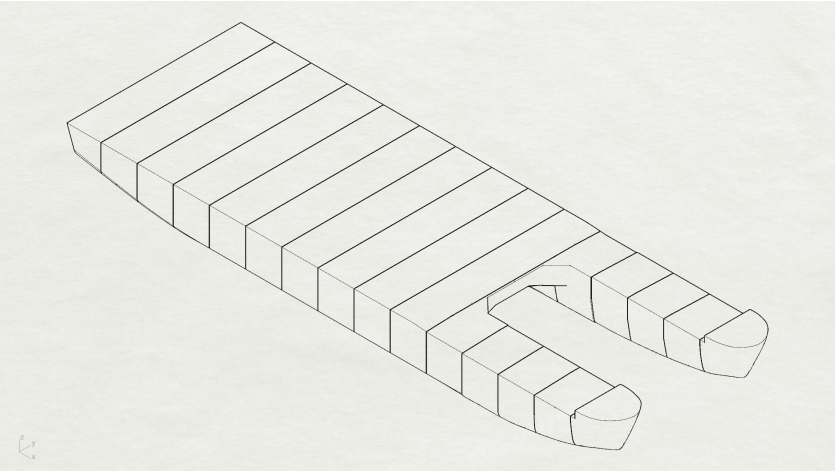

Figure 7.1: Example of a more efficient multi-body model

2. It is recommended to use one of the model order reduction techniques [2] from the field of structural dynamics to reduce the stiffness and mass matrix from the finite element model. In the current multi-body model stiffness of the vessel is approximated with a number of beam elements which have been tuned to match the natural frequencies from the finite element model. Only the first two structural modes were matched successfully. It is expected that a sophisticated model order reduction technique will lead to a more accurate approximation of the stiffness of the vessel.

3. The most important improvement for the multi-body model is to obtain the complete second order wave loads. At this moment the potential part of the second order wave loads is missing and it is expected that this part has a significant contribution to the second order wave loads. Taking into

account this potential part could lead to a better agreement between the second order hydroelastic response obtained with multi-body dynamics and the measured response.
It is recommended to use a hydrodynamic solver that can calculate the second order potential and calculates the potential part of the second order wave loads. Hydrostar could be used to obtain this potential part, because Hydrostar can calculate the second order potential [6] within a multi-body analysis.

Bibliography

[1] *Aqwa Theory Manual*. Ansys Inc., Canonsburg, PA 15317, January 2015.

[2] B. Besselink, U. Tabak, A. Lutowska, N. van de Wouw, H. Nijmeijer, D.J. Rixen, M.E. Hochstenbach, and W.H.A. Schilders. A comparison of model reduction techniques from structural dynamics, numerical mathematics and systems and control. *Journal of Sound and Vibration*, 332(19): 4403 – 4422, 2013. ISSN 0022-460X. doi: https://doi.org/10.1016/j.jsv.2013.03.025. URL http://www.sciencedirect.com/science/article/pii/S0022460X1300285X.

[3] R.E.D. Bishop and W.G. Price. *Hydroelasticity of Ships*. Cambridge University Press, 1979. ISBN 9780521223287. URL https://books.google.nl/books?id=6JzP7hBiZcQC.

[4] N Booij, Leo Holthuijsen, and R Ris. The "swan" wave model for shallow water. *Coastal Engineering*, 1, 01 1996.

[5] Rune Brincker, Lingmi Zhang, and Palle Andersen. Modal identification of output only systems using frequency domain decomposition. *Smart Materials and Structures*, 10:441, 06 2001. doi: 10.1088/0964-1726/10/3/303.

[6] *Hydrostar for experts, user manual*. Bureau Veritas, 92571 Neuilly-Sur-Seine, June 2016.

[7] X.B. Chen, B. Molin, and F. Petitjean. Numerical evaluation of the springing loads on tension leg platforms. *Marine Structures*, 8(5):501 – 524, 1995. ISSN 0951-8339. doi: https://doi.org/10.1016/0951-8339(95)97306-S. URL http://www.sciencedirect.com/science/article/pii/095183399597306S. Moored and Tethered Structures.

[8] YM Choi. *Second Order Hydroelastic Responses of a Vertical Circular Cylinder in Monochromatic Waves*. PhD thesis, MSc Thesis, Pusan National University, Korea, 2013.

[9] Roy R Craig Jr and Mervyn CC Bampton. Coupling of substructures for dynamic analyses. *AIAA journal*, 6(7):1313–1319, 1968.

[10] DNVGL. Dnvgl-rp-c205 environmental conditions and environmental loads. URL http://www.dnvgl.com.

[11] Klaus F Hasselmann, Tim P Barnett, E Bouws, H Carlson, David E Cartwright, K Eake, JA Euring, A Gicnapp, DE Hasselmann, P Kruseman, et al. Measurements of wind-wave growth and swell decay during the joint north sea wave project (jonswap). *Ergaenzungsheft zur Deutschen Hydrographischen Zeitschrift, Reihe A*, 1973.

[12] Kyeonguk Heo and Masashi Kashiwagi. A numerical study of second-order springing of an elastic body using higher-order boundary element method (hobem). *Applied Ocean Research*, 93: 101903, 2019. ISSN 0141-1187. doi: https://doi.org/10.1016/j.apor.2019.101903. URL http://www.sciencedirect.com/science/article/pii/S014111871830840X.

[13] S.E. Hirdaris, W.G. Price, and P. Temarel. Two- and three-dimensional hydroelastic modelling of a bulker in regular waves. *Marine Structures*, 16(8):627 – 658, 2003. ISSN 0951-8339. doi: https://doi.org/10.1016/j.marstruc.2004.01.005. URL http://www.sciencedirect.com/science/article/pii/S0951833904000061. P. Grundy.

[14] L.L. Huang and H.R. Riggs. The hydrostatic stiffness of flexible floating structures for linear hydroelasticity. *Marine Structures*, 13(2):91 – 106, 2000. ISSN 0951-8339. doi: https://doi.org/10.1016/S0951-8339(00)00007-1. URL http://www.sciencedirect.com/science/article/pii/S0951833900000071.

[15] Kazuhiro Iijima, Tetsuya Yao, and Torgeir Moan. Structural response of a ship in severe seas considering global hydroelastic vibrations. *Marine Structures*, 21(4):420 – 445, 2008. ISSN 0951-8339. doi: https://doi.org/10.1016/j.marstruc.2008.03.003. URL http://www.sciencedirect.com/science/article/pii/S0951833908000154.

[16] J.M.J. Journée, W.W. Massie, Faculty of Civil Engineering Delft University of Technology, Geosciences, R.H.M. Huijsmans, Maritime Delft University of Technology, Faculty of Mechanical, and Materials Engineering. *Offshore Hydromechanics*. TU Delft, 2000. URL https://books.google.nl/books?id=eN66jwEACAAJ.

[17] Dimitrios Konispoliatis and Spyridon Mavrakos. Mean drift forces on vertical cylindrical bodies placed in front of a breakwater. *Fluids*, 5:148, 08 2020. doi: 10.3390/fluids5030148.

[18] Da Lu, Shixiao Fu, Xiantao Zhang, Fei Guo, and Yun Gao. A method to estimate the hydroelastic behaviour of vlfs based on multi-rigid-body dynamics and beam bending. *Ships and Offshore Structures*, 14(4):354–362, 2019. doi: 10.1080/17445302.2016.1186332.

[19] . Malenica and J. Tuitman. 3dfem-3dbem model for springing and whipping analysis of ships. 2008.

[20] Šime Malenica, R Eatock Taylor, and JB Huang. Second-order water wave diffraction by an array of vertical cylinders. *Journal of Fluid Mechanics*, 390, 1999.

[21] Sime Malenica, Bernard Molin, Fabien REMY, and Ivo Senjanović. Hydroelastic response of a barge to impulsive and non-impulsive wave loads. *Hydroelasticity in Marine Technology*, 08 2003.

[22] Sime Malenica, Guillaume de Hauteclocque, igor ten, and Young-Myung Choi. Second order hydroelastic model of floating units. 10 2018.

[23] Miroslav Pastor, Michal Binda, and Tomáš Harčarik. Modal assurance criterion. *Procedia Engineering*, 48:543 – 548, 2012. ISSN 1877-7058. doi: https://doi.org/10.1016/j.proeng.2012.09.551. URL http://www.sciencedirect.com/science/article/pii/S1877705812046140. Modelling of Mechanical and Mechatronics Systems.

[24] J.A. Pinkster. *Low Frequency Second Order Wave Exciting Forces on Floating Structures*. Publication (Netherlands Scheepsbouwkundig Proefstation). Netherlands Ship Model Basin, 1980. URL https://books.google.nl/books?id=lvXYGwAACAAJ.

[25] Nils Salvesen, EO Tuck, and Odd Faltinsen. Ship motions and sea loads. 1970.

[26] Ivo Senjanović, Šime Malenica, and Stipe Tomas˘ević. Investigation of ship hydroelasticity. *Ocean Engineering*, 35(5):523 – 535, 2008. ISSN 0029-8018. doi: https://doi.org/10.1016/j.oceaneng.2007.11.008. URL http://www.sciencedirect.com/science/article/pii/S0029801807002545.

[27] Yan-Lin Shao and Odd M. Faltinsen. A numerical study of the second-order wave excitation of ship springing by a higher-order boundary element method. *International Journal of Naval Architecture and Ocean Engineering*, 6(4):1000 – 1013, 2014. ISSN 2092-6782. doi: https://doi.org/10.2478/IJNAOE-2013-0227. URL http://www.sciencedirect.com/science/article/pii/S2092678216302680.

[28] Yonggang Sun, Da Lu, Jin Xu, and Xiantao Zhang. A study of hydroelastic behavior of hinged vlfs. *International Journal of Naval Architecture and Ocean Engineering*, 10(2):170 – 179, 2018. ISSN 2092-6782. doi: https://doi.org/10.1016/j.ijnaoe.2017.05.002. URL http://www.sciencedirect.com/science/article/pii/S209267821630718X.

A

Theory: Modal decomposition

The modal decomposition introduced by Bishop and Price [3] is a widely used method to approach hydroelasticity. This method approaches the elastic behaviour of the vessel by describing it as a superposition of its modeshapes. The displacement of any point on the vessel is given by a time dependent part and a space dependent part, where the space dependent part comes from the modeshapes of the vessel:

$$X(\vec{x},t) = \sum_{j=1}^{N} \zeta_j e^{-\mathrm{i}\omega t} \delta_j(\vec{x}) \tag{A.1}$$

where X is the deformation anywhere on the vessel, N is the total number of modes taking into account, ζ_j is the modal amplitude and δ_j is the j^{th} dry modeshape. This method has been used by Senjanovic & Malenica in [26] to estimate the springing response of a flexible barge. The springing response of the vessel was estimated considering first order wave loads and showed good agreement with the measured response of the flexible barge.

Structural model

The hydroelastic model consists of a structural model and a hydrodynamic model. The structural model contains the structural mass and stiffness of the vessel. The structural model of the ship can be modelled as a three dimensional finite element model, but for beam-like hulls it can be convenient to use a one dimensional finite element model. The dry natural frequencies and modes of the structural model can be obtained by solving the following matrix equation:

$$([\mathbf{K}] - \omega^2[\mathbf{M}])\{\delta\} = \{0\} \tag{A.2}$$

Where $[\mathbf{K}]$ is the stiffness matrix and $[\mathbf{M}]$ is the mass matrix, both coming from the finite element model. By solving the dry natural modes of the structural model, a natural modes matrix can be constituted:

$$[\delta] = [\{\delta\}_1, \{\delta\}_2, \ldots, \{\delta\}_N] \tag{A.3}$$

Where N is the total number of modes that is taken into account. The matrix containing the dry modes $[\delta]$ is then used to determine the modal mass and modal stiffness:

$$[K] = [\delta]^T[\mathbf{K}][\delta], \quad [M] = [\delta]^T[\mathbf{M}][\delta] \tag{A.4}$$

The modal mass and stiffness matrix are of size N-by-N, where N is the total number of modes taking into account. For example, if the first two structural modes are taken into account the total number of modes becomes 8. This is because the first 6 modes represent the rigid body modes, respectively surge, sway, heave, roll, pitch and yaw.

Geometrical model of the wetted surface

The geometrical model contains the geometry of the wetted surface. The wetted surface of the hull is divided into panels. The dry modes of the structural model are transferred to the panel model. There are several methods to map the dry modes of the structural model on to the panel model depending on the dimensions of the model. The dry modeshape mapped on the panel model is noted by h_j.
The deformation of the panel model, so the outer hull, is presented as:

$$H(\vec{x},t) = \sum_{j=1}^{N} \zeta_j e^{-\mathrm{i}\omega t} h_j(\vec{x}) \tag{A.5}$$

where $H(\vec{x},t)$ is the vector for the deformation of the panel model, ζ_j is the modal amplitude and $h_j(\vec{x})$ is a vector containing the j^{th} dry modeshape transferred from the structural model to the panel model.

In order to solve for the modal amplitudes, the forces acting on the structure need to be determined. First, the fluid around the structure should be described. The hydroelastic model uses potential theory to describe the fluid domain. The potential theory uses the velocity potential function $\phi(\vec{x},t)$, which is defined as a function of which the spatial derivatives are equal to the velocity of the water particles.

$$u_x = \frac{\partial \phi}{\partial x}, \quad u_y = \frac{\partial \phi}{\partial y}, \quad u_z = \frac{\partial \phi}{\partial z} \tag{A.6}$$

In order to solve for the potential function, a number of boundary conditions is set up. Within the fluid domain, the potential must fulfill the Laplace equation:

$$\frac{\partial^2 \phi}{\partial x^2} + \frac{\partial^2 \phi}{\partial y^2} + \frac{\partial^2 \phi}{\partial z^2} = 0 \tag{A.7}$$

At the mean free surface $(z = 0)$ the next boundary condition needs to be satisfied. This boundary condition is a combination of a dynamic boundary condition and a kinematic boundary condition. The kinematic boundary condition ensures that water particles at the free surface do not leave the free surface. The dynamic boundary condition ensures that the pressure at the water surface is constant.

$$\frac{\partial^2 \phi}{\partial t^2} + g\frac{\partial \phi}{\partial z} = 0 \tag{A.8}$$

The body boundary condition is a no-leak condition, which means that the fluid doesn't penetrate through the wetted surface of the body. This can be described as:

$$\frac{\partial \phi}{\partial n} = \frac{\partial H}{\partial t} \cdot \vec{n} \quad \text{on the wetted surface S} \tag{A.9}$$

where $\vec{n}$ is the normal vector of the wetted surface. It is assumed that the velocity potential function is periodic with frequency ω, which means that velocity potential function can be described as:

$$\phi(\vec{x},t) = Re\{\varphi(\vec{x})e^{-i\omega t}\} \tag{A.10}$$

According to Salvesen [25] the potential φ can be decomposed into an incident potential, a diffracted potential and the radiation potentials:

$$\varphi = \varphi_I + \varphi_D - \mathrm{i}\omega \sum_{j=1}^{N} \zeta_j \varphi_{Rj} \tag{A.11}$$

The incident wave potential is known analytically and given by:

$$\varphi_I = -\mathrm{i}\frac{g\eta_a}{\omega} e^{k(z+\mathrm{i}x)} \tag{A.12}$$

where η_a is the wave amplitude and k is the wave number. The diffraction potential is the incident wave potential diffracted by the body. The radiation potentials are the potentials from the oscillary motions

of the body in still water. By decomposing the velocity potential, the body boundary conditions can be rewritten to:

$$\frac{\partial \varphi_D}{\partial n} = -\frac{\partial \varphi_I}{\partial n}, \quad \frac{\partial \varphi_{Rj}}{\partial n} = h_j \cdot \vec{n} \tag{A.13}$$

Once the potentials are determined, the forces acting on the structure can be determined by integrating the pressure over the wetted surface. The pressure is obtained by the Bernoulli equation:

$$p = -\rho g z - \rho \frac{\partial \phi}{\partial t} - \frac{1}{2}\rho(\vec{\nabla}\phi)^2 \tag{A.14}$$

In the first order hydroelastic model, we are interested in the first order wave loads, so the linearized Bernoulli equation is used:

$$p = -\rho g z + \mathrm{i}\omega\rho\phi \tag{A.15}$$

Furthermore, to obtain the modal first order wave loads the pressure should be integrated over the mean constant wetted surface.

$$F_j = \iint_S p \cdot h_j \cdot \vec{n} \cdot dS \tag{A.16}$$

The modal forces can be split into a hydrostatic part and a hydrodynamic part.

$$F_j = -\iint_S \rho g z \cdot h_j \cdot \vec{n} \cdot dS + \iint_S \mathrm{i}\omega\rho\phi \cdot h_j \cdot \vec{n} \cdot dS \tag{A.17}$$

Hydrodynamic loads

First the hydrodynamic loads will be derived. Because the velocity potential is periodic with frequency ω, the hydrodynamic load is also periodic with frequency ω. The modal hydrodynamic load can thus be written as:

$$F_j^{HD} = F_{ja}^{HD} e^{-\mathrm{i}\omega t} \tag{A.18}$$

where F_{ja}^{HD} represents the amplitude of the modal hydrodynamic load. Substituting equation A.11 into the hydrodynamic part of equation A.17 leads to the following formulation for the amplitude of the modal hydrodynamic load:

$$F_{ja}^{HD} = \mathrm{i}\omega\rho \iint_S (\varphi_I + \varphi_D) \cdot h_j \cdot \vec{n} \cdot dS + \omega^2 \rho \sum_{j=1}^{N} \zeta_j \iint_S \varphi_{Rj} \cdot h_j \cdot \vec{n} \cdot dS \tag{A.19}$$

This amplitude is split into a excitation part and a radiation part.

$$\begin{aligned} F_j^{DI} &= \mathrm{i}\omega\rho \iint_S (\varphi_I + \varphi_D) \cdot h_j \cdot \vec{n} \cdot dS \\ F_j^{R} &= \omega^2 \rho \sum_{j=1}^{N} \zeta_j \iint_S \varphi_{Rj} \cdot h_j \cdot \vec{n} \cdot dS \end{aligned} \tag{A.20}$$

The radiation part F_j^R can be decomposed into a real and imaginary part, representing the modal inertia force and the damping force:

$$\begin{aligned} Re(F_j^R) &= \omega^2 \sum_{i=1}^{N} \zeta_i A_{ij} \\ A_{ij} &= \rho Re\left\{ \iint_S \varphi_{Ri} \cdot h_j \cdot \vec{n} \cdot dS \right\} \\ i \cdot Im(F_j^R) &= \mathrm{i}\omega \sum_{i=1}^{N} \zeta_i B_{ij} \\ B_{ij} &= \rho\omega Im\left\{ \iint_S \varphi_{Ri} \cdot h_j \cdot \vec{n} \cdot dS \right\} \end{aligned} \tag{A.21}$$

Hydrostatic loads
The hydrostatic load can be written as a function of the modal amplitude and a restoring coefficient:

$$F_j^C = -\sum_{i=1}^{N} \zeta_i C_{ij} \tag{A.22}$$

The full derivation for the restoring coefficient can be found in [26].

Equation of motion
The equation of motion can be constructed using Newton's second law:

$$F = ma \tag{A.23}$$

First, let's construct the equation of motion in modal space for the structural model. In order to do this the modal mass matrix and the modal stiffness matrix are required. As mentioned earlier it is assumed that the motion is periodic with frequency ω. The modal equation of motion for the structural model can then be described as a function of the modal amplitudes ζ_j.

$$-\omega^2[M]\vec{\zeta}e^{-\mathrm{i}\omega t} = -[K]\vec{\zeta}e^{-\mathrm{i}\omega t} \tag{A.24}$$

where $\vec{\zeta}$ is a vector containing the modal amplitudes for each mode j, $\vec{\zeta} = \{\zeta_1, \zeta_2, \ldots \zeta_N\}$. Now the modal equation of motion can be extended with the modal hydrodynamic loads and the modal hydrostatic loads. Note that the loads are also time periodic with frequency ω, so the time periodicity is left out of the equation.

$$\begin{aligned}
&(-\omega^2[M] + [K])\vec{\zeta} = \vec{F}^{DI} + \vec{F}^{R} + \vec{F}^{C} \\
&(-\omega^2[M] + [K])\vec{\zeta} = \omega^2[A]\vec{\zeta} + \mathrm{i}\omega[B]\vec{\zeta} - [C]\vec{\zeta} + \vec{F}^{DI} \\
&\{(-\omega^2([M] + [A]) - \mathrm{i}\omega[B] + [K] + [C]\}\vec{\zeta} = \vec{F}^{DI}
\end{aligned} \tag{A.25}$$

The above equation can be solved for the modal amplitudes and can be substituted into equation A.1 to obtain the deformation due to first order wave loads at any location of the structure. The local velocity and local acceleration follow from the local deformation.

$$\begin{aligned}
&X(\vec{x}, t) = \sum_{j=1}^{N} \zeta_j e^{-\mathrm{i}\omega t}\delta_j(\vec{x}) \\
&\frac{\partial X(\vec{x}, t)}{\partial t} = -\mathrm{i}\omega \sum_{j=1}^{N} \zeta_j e^{-\mathrm{i}\omega t}\delta_j(\vec{x}) = -\mathrm{i}\omega X(\vec{x}, t) \\
&\frac{\partial^2 X(\vec{x}, t)}{\partial t^2} = -\omega^2 \sum_{j=1}^{N} \zeta_j e^{-\mathrm{i}\omega t}\delta_j(\vec{x}) = -\omega^2 X(\vec{x}, t)
\end{aligned} \tag{A.26}$$

B

Full-scale measurements

C

Benchmark study

A benchmark study is performed using AQWA to ensure that the method based on multi-body dynamics is applied in the right matter and to discover the limitations of the software. For example, the total number of interacting structures that can be defined in AQWA is 20. This is an important limitation that needs to be taken into account when modelling a multi-body model of Pioneering Spirit.
The experiments from Malenica in [21] will be used to validate that the method is applied in the right manner. In the experiments a barge is modelled with 12 pontoons connected to each other with two elastic plates as can be seen in figure C.1. The dimensions of the barge are given in table C.1.

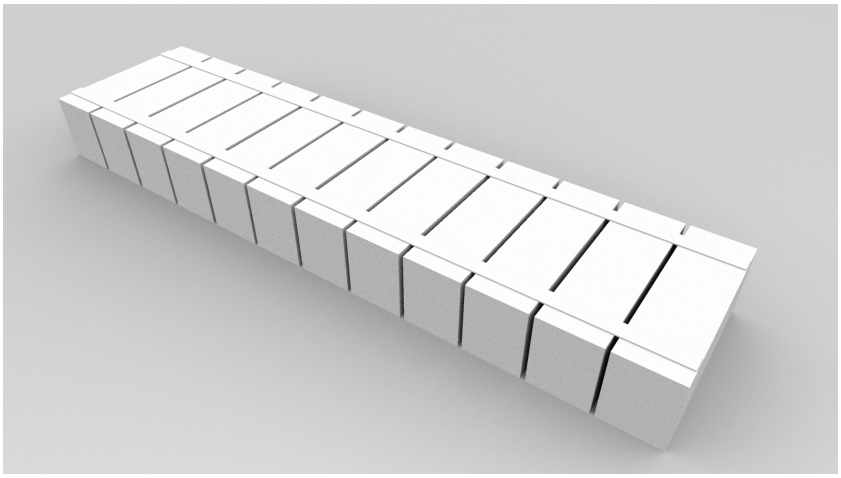

Figure C.1: 12 pontoons connected with two elastic plates

Table C.1: Dimensions of the barge

Pontoon length	0.19 m
Barge length	2.445 m
Width	0.6 m
Height	0.25 m
Depth	0.12 m
Height elastic plates	4 mm
Width elastic plates	50 mm

C.1. Transforming stiffness matrix

Each pontoon is modelled into AQWA as an individual structure. Next, the stiffness matrices of the beam elements is defined in AQWA. The stiffness matrix needs to be defined at the centre of gravity

of each pontoon, so the stiffness matrices from the elastic plates are first transformed to the centre of gravity of each pontoon. This can be explained with the help of figure C.2. The stiffness matrix of the beam element is given at the location of the elastic plates and describes the relation between the forces and displacements in nodes i and j:

$$\begin{Bmatrix} F_i \\ F_j \end{Bmatrix} = [K_e] \begin{Bmatrix} \eta_i \\ \eta_j \end{Bmatrix} \tag{C.1}$$

The displacements at nodes i and j, η_i, η_j, can be described as a function of the displacements of the centres of gravity, η_i', η_j'.

$$\begin{Bmatrix} \eta_i \\ \eta_j \end{Bmatrix} = \begin{bmatrix} T_i & 0 \\ 0 & T_j \end{bmatrix} \begin{Bmatrix} \eta_i' \\ \eta_j' \end{Bmatrix} \tag{C.2}$$

The forces acting in the centres of gravity, F_i', F_j', can be described as a function of the forces in nodes i and j with the same transformation matrices:

$$\begin{Bmatrix} F_i' \\ F_j' \end{Bmatrix} = \begin{bmatrix} T_i^T & 0 \\ 0 & T_j^T \end{bmatrix} \begin{Bmatrix} F_i \\ F_j \end{Bmatrix} \tag{C.3}$$

The above equations can now be used to describe the relation between the forces and displacements in the centres of gravity:

$$\begin{aligned} \begin{Bmatrix} F_i' \\ F_j' \end{Bmatrix} &= \begin{bmatrix} T_i^T & 0 \\ 0 & T_j^T \end{bmatrix} \begin{Bmatrix} F_i \\ F_j \end{Bmatrix} \\ \begin{Bmatrix} F_i' \\ F_j' \end{Bmatrix} &= \begin{bmatrix} T_i^T & 0 \\ 0 & T_j^T \end{bmatrix} [K_e] \begin{Bmatrix} \eta_i \\ \eta_j \end{Bmatrix} \\ \begin{Bmatrix} F_i' \\ F_j' \end{Bmatrix} &= \begin{bmatrix} T_i^T & 0 \\ 0 & T_j^T \end{bmatrix} [K_e] \begin{bmatrix} T_i & 0 \\ 0 & T_j \end{bmatrix} \begin{Bmatrix} \eta_i' \\ \eta_j' \end{Bmatrix} \end{aligned} \tag{C.4}$$

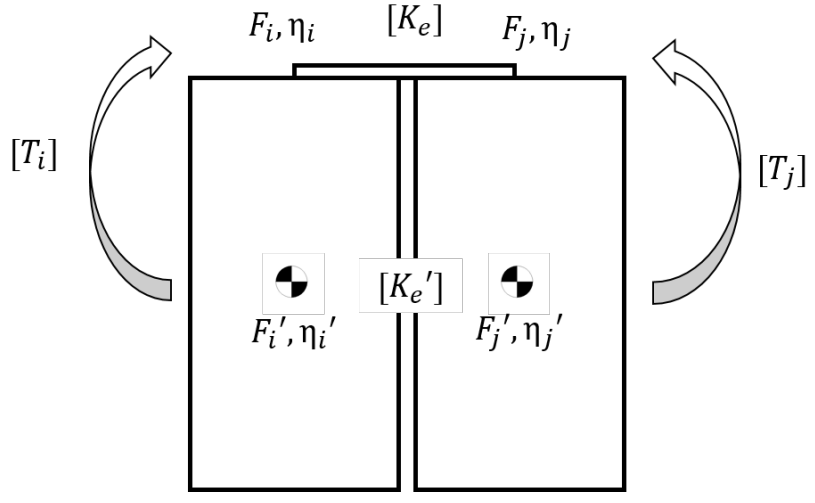

Figure C.2: Illustration of how to transform the stiffness matrix

The stiffness matrix of the connecting beam elements is defined in AQWA. Figures C.3 and C.4 show the multi-body analysis without and with the connecting stiffness matrices. It can be seen that when the stiffness matrices are applied, the pontoons behave as a continuous barge.

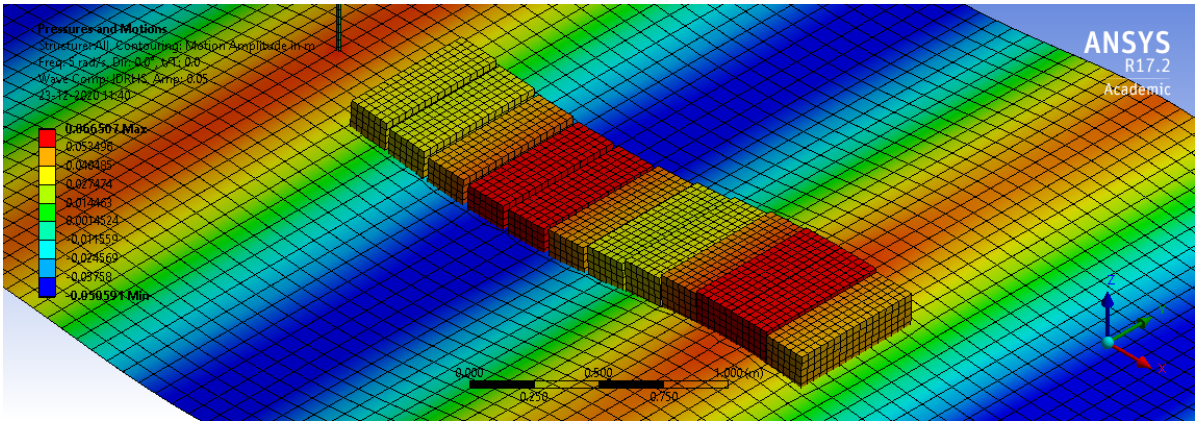

Figure C.3: Multi-body analysis without connecting stiffness matrices

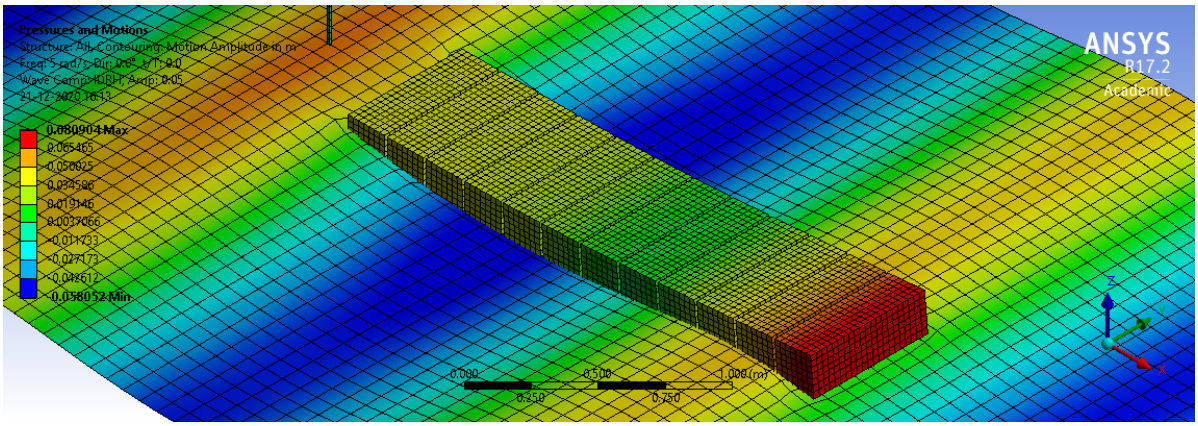

Figure C.4: Multi-body analysis with connecting stiffness matrices

C.2. Response Amplitude Operators

The response amplitude operators for each pontoon can be obtained with the multi-body analysis. These can be compared with the experimental values in [21]. The response amplitude operators have also been approached by Malenica using modal decomposition. The RAO's for the heave motion for the first and seventh pontoon are given in figures C.5 and C.6. These figure include the results from the multi-body analysis, modal decomposition and the experiments. It can be seen that the multi-body analysis shows good agreements with the experimental values and the results coming from modal decomposition.

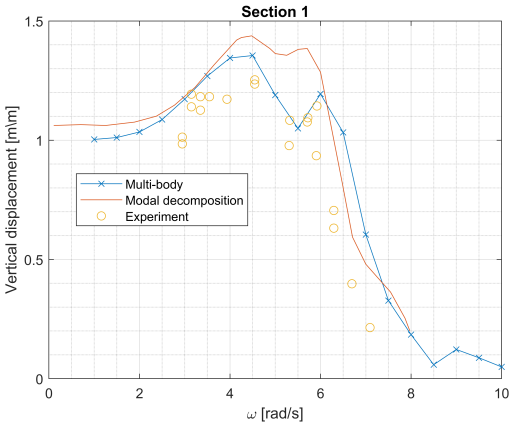

Figure C.5: Vertical displacement section 1

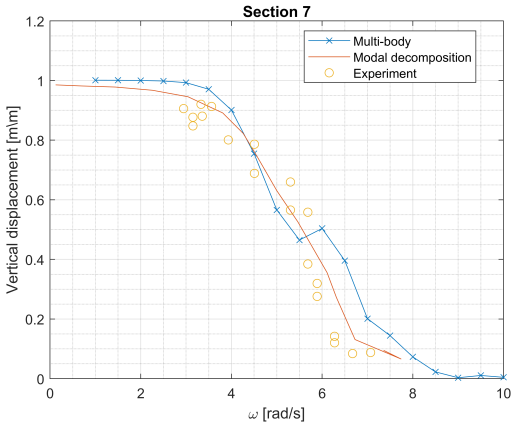

Figure C.6: Vertical displacement section 7

D

Stiffness matrix beam elements

The stiffness matrix of a beam element describes the relation between the forces applied at the outer ends of the beam and the displacements and rotations of these outer ends. The coordinate system of the beam element is given in figure D.2. The stiffness matrix of the beam element based on Timoshenko beam theory is given by:

$$[Ke] = \begin{bmatrix}
\frac{EA}{L} & & & & & & & & & & & \\
0 & \frac{12EI_z}{L^3(1+\beta_y)} & & & & & & & & & & \\
0 & 0 & \frac{12EI_y}{L^3(1+\beta_z)} & & & & & & & & & \\
0 & 0 & 0 & \frac{GI_t}{L} & & & & & & & & \\
0 & 0 & \frac{-6EI_y}{L^2(1+\beta_z)} & 0 & \frac{(4+\beta_z)EI_y}{L(1+\beta_z)} & & & & & & & \\
0 & \frac{6EI_z}{L^2(1+\beta_y)} & 0 & 0 & 0 & \frac{(4+\beta_y)EI_z}{L(1+\beta_y)} & & & & & & \\
\frac{-EA}{L} & 0 & 0 & 0 & 0 & 0 & \frac{EA}{L} & & & & & \\
0 & \frac{-12EI_z}{L^3(1+\beta_y)} & 0 & 0 & 0 & \frac{-6EI_z}{L^2(1+\beta_y)} & 0 & \frac{12EI_z}{L^3(1+\beta_y)} & & & & \\
0 & 0 & \frac{-12EI_y}{L^3(1+\beta_z)} & 0 & \frac{6EI_y}{L^2(1+\beta_z)} & 0 & 0 & 0 & \frac{12EI_y}{L^3(1+\beta_z)} & & & \\
0 & 0 & 0 & \frac{-GI_t}{L} & 0 & 0 & 0 & 0 & 0 & \frac{GI_t}{L} & & \\
0 & 0 & \frac{-6EI_y}{L^2(1+\beta_z)} & 0 & \frac{(2-\beta_z)EI_y}{L(1+\beta_z)} & 0 & 0 & 0 & \frac{6EI_y}{L^2(1+\beta_z)} & 0 & \frac{(4+\beta_z)EI_y}{L(1+\beta_z)} & \\
0 & \frac{6EI_z}{L^2(1+\beta_y)} & 0 & 0 & 0 & \frac{(2-\beta_y)EI_z}{L(1+\beta_y)} & 0 & \frac{-6EI_z}{L^2(1+\beta_y)} & 0 & 0 & 0 & \frac{(4+\beta_y)EI_z}{L(1+\beta_y)}
\end{bmatrix}$$

$symmetry$

The stiffness matrix of multiple connected beam elements can be constructed by superposition of the overlapping nodes. For example, the total stiffness matrix of the situation given in figure D.1 would become:

$$K_s = \begin{bmatrix} k_{ii} & k_{ij} & 0 \\ k_{ji} & 2k_{jj} & k_{jk} \\ 0 & k_{kj} & k_{kk} \end{bmatrix} \tag{D.1}$$

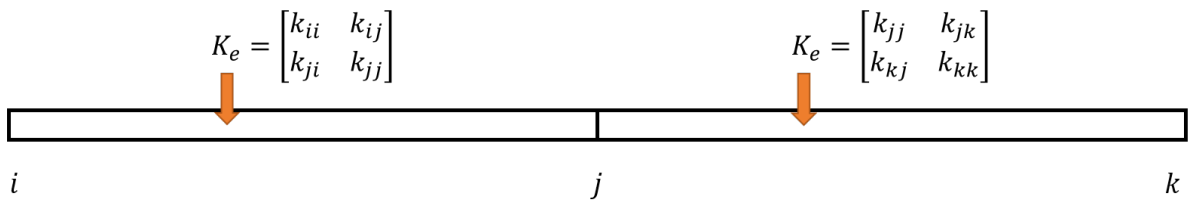

Figure D.1: Connecting beam elements

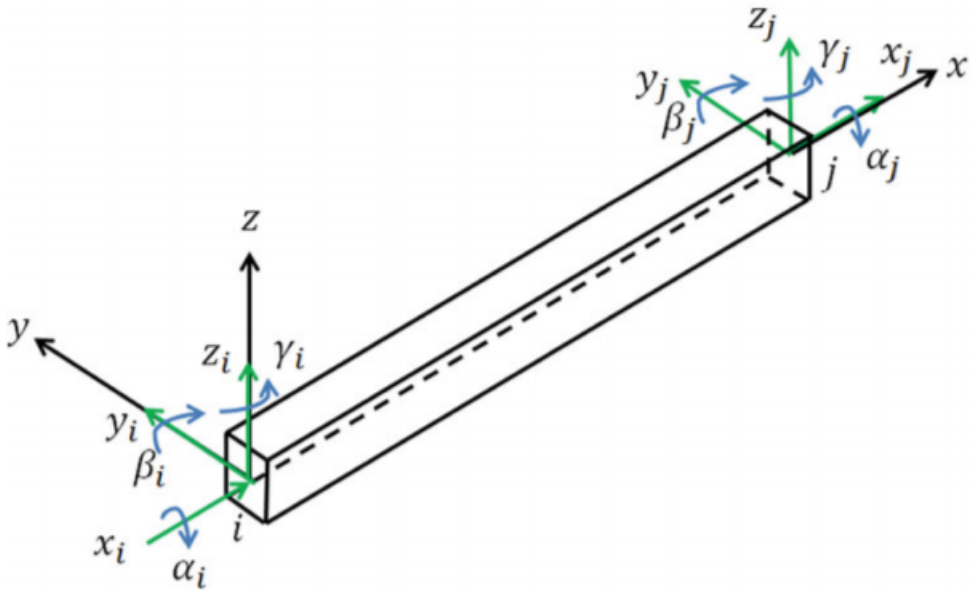

Figure D.2: Beam element